CONFIDENTIAL

NASA TM X-540

TECHNICAL MEMORANDUM

X-540

AN INVESTIGATION OF MODIFIED CLUSTERED JET-EXIT ARRANGEMENTS AT SUPERSONIC SPEEDS

By Harry T. Norton, Jr., Willard E. Foss, Jr., and John M. Swihart

Langley Research Center
Langley Field, Va.

NATIONAL AERONAUTICS AND SPACE ADMINISTRATION
WASHINGTON
July 1961

CONFIDENTIAL

CONFIDENTIAL

NATIONAL AERONAUTICS AND SPACE ADMINISTRATION

TECHNICAL MEMORANDUM X-540

AN INVESTIGATION OF MODIFIED CLUSTERED JET-EXIT ARRANGEMENTS AT SUPERSONIC SPEEDS*

By Harry T. Norton, Jr., Willard E. Foss, Jr., and John M. Swihart

SUMMARY

An investigation of several side-by-side modified clustered jet-exit configurations has been conducted in the Langley 9- by 12-inch supersonic blowdown tunnel at Mach numbers from 1.62 to 3.05. The semi-span models were mounted from the tunnel wall and three jet exhausts were simulated with cold air. The angle of attack was maintained at 0° and the Reynolds number range was 7×10^6 to 11×10^6 based on model wing root chord.

The results of the investigation indicate that larger gains in performance were obtained by eliminating large flat base areas with terminal fairings than by boattailing between nacelles. The results also indicate some possible improvement in performance by careful nozzle-slot design.

INTRODUCTION

Large supersonic airplanes may have a number of engines grouped together in a side-by-side arrangement. For such configurations, interference of the multiple jets on the afterbodies, bases, and fairings between engines would be expected to have important effects on the airplane performance. Some results obtained with side-by-side clustered exit arrangements at supersonic speeds are shown in references 1 and 2. Results presented in references 3 and 4 indicate that an improvement in off-design performance might be obtained by slotting the nozzle afterbody or by adding terminal fairings. However, the use of modified

*Title, Unclassified.

nozzles to obtain improved off-design performance may seriously affect the on-design range of a $M = 3.0$ cruise airplane.

The purpose of the paper is to present data obtained at supersonic speeds in the Langley 9- by 12-inch supersonic blowdown tunnel on several modified clustered exit arrangements. The semispan model simulated a propulsion system mounted below the wing with the center of the jet exits at the wing trailing edge. The exit modifications included slotted-nozzle afterbodies and terminal fairings. The jet flow was simulated with cold air at jet total-pressure ratios from 1 (jet off) to about 40 at Mach numbers of 1.62, 1.96, 2.55, and 3.05. The Reynolds number range was from about 7×10^6 to 11×10^6 based on model wing root chord.

SYMBOLS

d diameter

C_D drag coefficient, D/qS

$C_{D,i}$ jet-off drag coefficient of the model with configuration 8 having the pressures on the base and jet-exit areas adjusted to free-stream static pressure

C_F thrust coefficient, F/qS

$C_{F,i}$ ideal thrust coefficient, F_i/qS

C_p pressure coefficient, $\dfrac{p_l - p_\infty}{q}$

D drag

F thrust

F_i ideal jet thrust for complete isentropic expansion to free-stream static pressure, $w\sqrt{\dfrac{2R}{g}\dfrac{\gamma}{\gamma - 1}T_{t,j}\left[1 - \left(\dfrac{p_\infty}{p_{t,j}}\right)^{\frac{\gamma-1}{\gamma}}\right]}$

g acceleration of gravity

l nozzle length from throat to exit

M	Mach number
N_{Re}	Reynolds number
p	pressure
$p_{t,j}/p_\infty$	ratio of jet total pressure to free-stream static pressure
q	dynamic pressure
R	gas constant, ft/°R
S	wing area (0.35 sq ft)
T_t	stagnation temperature
w	weight flow
x	distance from wing trailing edge (positive rearward)
β	boattail angle
γ	ratio of specific heats
η	efficiency factor, $(C_F - C_D + C_{D,i})/C_{F,i}$
θ	nozzle divergence angle

Subscripts:

av	average
b	base
e	exit
i	ideal
j	jet
l	local
max	maximum
p	nozzle throat

t total

∞ free stream

APPARATUS AND METHODS

Models

The general jet-exit test arrangement is presented in figure 1 and is identical to that used in reference 2. Photographs of the model are shown in figure 2 and the geometric details are shown in figure 3. The wing of the model was of a smaller scale than the engines to permit investigation of larger scale exits than would be possible with a true semispan model in the Langley 9- by 12-inch supersonic blowdown tunnel; however, the coefficients presented herein are based on the wing area of a true semispan model (0.35 sq ft) which is scaled according to exit size to give the drag coefficients realistic values. Details of the exit configurations are shown in figure 4 and table I. The same configuration numbers have been retained in this paper that were used in reference 2 since the present configurations are modifications to the originals. Photographs of the configurations are shown in figure 5.

Configuration 5 was modified by cutting longitudinal slots in the nozzle diverging section in a manner similar to that shown in reference 3 for the slotted-afterbody model. One set of slots (called short slots) extended 50 percent of the distance from the exit to the throat and the second set of slots (called long slots) extended from the exit to the throat. The short and long slots eliminated about 14 and 21 percent, respectively, of the surface area of the divergent portion of the nozzle. These slots provided a means for ventilating the nozzle with free-stream air. (See ref. 3.)

Configuration 8 was modified with afterbody terminal fairings designed according to the concepts presented in reference 4. These afterbody terminal fairings eliminate the flat base area and provide thrust surfaces for the underexpanded jet. (See fig. 4(c).)

Configuration 9 was modified in a manner similar to that used on configuration 5. The slots extended about 60 percent of the distance from the exit to the throat and eliminated about 10 percent of the nozzle surface area.

Tests and Measurements

The investigation was conducted in the Langley 9- by 12-inch supersonic blowdown tunnel concurrently with that of reference 2. The stagnation pressures ranged from 35 to 50 lb/sq in. abs for Mach numbers of 1.62, 1.96, 2.55, and 3.05 and these Mach numbers were obtained by using interchangeable nozzle blocks. The Reynolds number, based on a model wing root chord of 10 inches, ranged from 7×10^6 to 11×10^6, depending upon the test Mach number and stagnation pressure. The investigation was conducted at an angle of attack and an angle of yaw of 0°.

The jet-exit air flow was furnished from a 300 lb/sq in. abs supply and was conducted to the model through the center of the strain-gage balance, as shown in figure 1. The air flow was turned 90° upon entering the model and was exhausted axially through the three jet exits (fig. 1(b)). Jet total pressure was controlled by a mechanical pressure-regulator valve and the value obtained from a total-pressure tube installed on the center line of each duct upstream of the throat (fig. 4(a)). The total jet weight flow was determined by a calibrated Venturi meter.

Surface pressure orifices were located on configuration 5 as shown in figure 4 and they were used to determine the local pressure coefficients over the fairing section between nacelles. For configurations 8 and 9 from 6 to 12 surface pressure orifices were spaced in the base area to determine base pressure coefficients. For configuration 8 with the terminal fairings two orifices were located on the inner surface of one of the fairings (fig. 4(c)) to determine the local pressures on the fairings during jet operation.

Model forces and moments were determined by a three-component strain-gage balance with a hollow center which was attached to the tunnel top, as shown in figure 1(b). The normal-force and pitching-moment outputs of the three-component balance were used to correct the axial-force output for interactions, and only axial-force data are presented in this paper. As mentioned previously, jet air was piped through the center of the balance to the model. The supply piping arrangement shown in figure 1 was selected to minimize force-interference effects between the model and the supply pipe supports. Calibration of the balance with and without the supply pipe installed showed no effects of the pipe on the forces and moments within the accuracy of the measurements.

Installation of the model through the tunnel wall required a clearance gap of 1/16 inch between the model and wall to avoid balance fouling (fig. 3). Because of the large pressure differential existing between the atmosphere and the tunnel stream during operation at the higher Mach numbers, leakage flow through the gap and into the tunnel could cause significant interference effects on the measured forces. In order to

avoid these interference effects, a cylindrical shroud, the top of which was formed into a labyrinth seal, was installed around the balance. (See fig. 1(b).)

All pressure, temperature, and force data were recorded simultaneously for each individual test point. Pressures were recorded on film using diaphragm-type pressure cells. The forces, moments, and jet total temperature were determined from the outputs of self-balancing potentiometers which were recorded on strip charts. The accuracy of measurement is estimated to be as follows:

M	± 0.02
N_{Re}, percent, caused by changes in T_t	± 0.01
T_t, $^{\circ}R$	± 2
$p_{t,j}/p_{\infty}$	± 0.4
C_D	± 0.001
C_F	± 0.001
C_p	± 0.01

RESULTS AND DISCUSSION

Jet Simulation

Jet-exit flow for the present configurations was obtained by using room-temperature air. As pointed out in reference 5, the wave interference of a hot jet operating at or above the design-pressure ratio can be closely simulated with a cold jet if the initial slope of the jet boundary is duplicated. Duplication of the initial slope of the jet boundary is accomplished by operating the cold jet ($\gamma = 1.4$) at higher total-pressure ratios. The total-pressure-ratio variation with Mach number of a typical operating supersonic turbojet engine is shown in figure 6. The total-pressure-ratio variation of a cold jet which produces approximately the same initial jet boundary as that produced by the hot turbojet engine is also shown in figure 6. Analysis figures presented in this paper are presented at the scheduled cold-air pressure ratios.

Basic Data

The variation of measured thrust-minus-drag coefficient with jet total-pressure ratio for the configurations is shown in figure 7 at Mach numbers of 1.62, 1.96, 2.55, and 3.05. The value of $C_T - C_D$

plotted at a jet total-pressure ratio of 1.0 represents the jet-off drag of the configuration.

Pressure distributions over the fairing between the nacelle are shown in figure 8 for configuration 5 with long slots. Increasing the jet total-pressure ratio produced more positive pressures on the fairing down stream of the nozzle throat which is located at $x = -0.543$. Pressure distributions over the fairing between the nacelles were not obtained on configurations 8 and 9.

Base Pressure

The variation of the arithmetically averaged base pressure coefficient with jet total-pressure ratio for configuration 8 with and without terminal fairings is shown in figure 9. It can be seen that the effect of the terminal fairings on the average base pressure coefficient varied with both jet total-pressure ratio and free-stream Mach number. In general, the base pressure coefficients were reduced (became more negative) by the addition of the fairings at the lower Mach numbers and increased at the higher Mach numbers. Also, the variation of the pressure coefficient on the inside surface of the terminal fairing is shown in figure 9. It is apparent that the jet was expanding against the terminal fairing surface, producing much more favorable levels of pressure coefficient at the higher pressure ratios and is very beneficial at $M = 3.05$.

The variation of the average base pressure coefficient with pressure ratio is shown in figure 10 for configuration 9 and for configuration 9 slotted. In general, the effect of the slots was to produce slightly more positive base pressure at the lower pressure ratios and more negative base pressure at the higher pressure ratios. This result at the lower pressure ratios is due to the ventilating effect of the slots while at the higher pressure ratios the slots eliminated the beneficial interference effects associated with a solid nozzle.

The variation of base pressure coefficient with Mach number at the scheduled jet total-pressure ratio is shown in figure 11 for configuration 8 and in figure 12 for configuration 9. The terminal fairing surfaces on configuration 8 are shown to be experiencing thrust forces at Mach numbers above 2.2 in figure 11. These positive pressure forces will be shown later to have a very beneficial effect on the net thrust minus drag of the configuration. The data presented in figure 12 indicate that the slot used on configuration 9 had a detrimental effect on the base pressure at all Mach numbers except $M = 3.05$.

Performance

The effect of Mach number on configuration efficiency factor η is shown in figure 13 for the configurations. Configuration efficiency factor η is defined as the measured thrust minus drag of the model plus the installation drag of the model divided by the ideal thrust of a nozzle passing the same airflow as the configuration being considered. Installation drag is the jet-off drag of the model with the zero boattail flat base configuration (configuration 8 with the entire base region adjusted to free-stream static pressure). In this manner, the change in thrust or drag due to the various modifications is reflected as an increase or decrease in configuration efficiency factor.

As stated previously, configuration 5 was modified by slotting the divergent portion of the nozzle. The effect of these modifications is shown in figure 13(a). In general, the effect of slotting the nozzle was not as might be expected. For example at $M = 1.62$, the long slots produced a loss in η even though the pressure distributions presented in figure 8 indicated possible drag reductions. The loss in η is therefore due to thrust losses associated with the jet expanding through the long slots. At Mach number 2.52 where the nozzle is on design pressure ratio, both of the slotted nozzles had better performance than the solid nozzle indicating that the reduction in drag was greater than the loss in thrust due to the slots. At $M = 3.05$ there was little difference in the long and short slots, both of them are about 10 percent lower in η than the solid nozzle. This large loss is probably due to flow through the slots and consequent loss in internal thrust. The short slots were better than the long slots at the lower Mach numbers.

The results presented in figure 13(b) indicate the effect of slots on the performance of configuration 9. As stated previously the area of the slots was less than those used on configuration 5. It can be seen that reducing the area of the slots eliminated most of the thrust losses at $M = 1.62$ (configuration 5, long slots) but did not provide the improvement associated with the slots of configuration 5 at the higher Mach numbers. In general the results presented in figure 13(a) and (b) indicate some possible improvements in performance, by careful nozzle-slot design.

Configuration 8 with and without terminal fairings is compared in figure 13(c) to show the effect of eliminating large flat base area by using terminal fairings. Configuration 1 from reference 2 is compared to configuration 8 in figure 13(c) and shows the effect of eliminating base area by boattailing. Configuration 1 has the same internal nozzle geometry as configuration 8; however, the fairing between the engine afterbodies was the same as configuration 5 and the engine afterbodies were boattailed ($\beta = 6.9^\circ$). The results indicate that large gains in performance were obtained by eliminating large flat base areas with

terminal fairings and by boattailing between nacelles. Of primary interest in figure 13(c) is the fact that, at the higher Mach numbers larger gains in performance were obtained by terminal fairings than by boattailing. The jet is operating well above design pressure ratio $\left(p_{t,j}/p_{\infty} = 7.7, \quad \gamma = 1.4\right)$ and the positive pressures of the under expanded jet are acting along the terminal fairings thereby producing thrust. (See fig. 11.)

CONCLUDING REMARKS

An investigation of modified clustered jet-exit configurations arranged side by side along the trailing edge of a wing has been conducted in the Langley 9- by 12-inch supersonic blowdown tunnel at Mach numbers of 1.62, 1.96, 2.55, and 3.05. The results of the investigation indicate that significant gains in performance were obtained by eliminating large flat base areas with terminal fairings and by boattailing between nacelles. For one specific configuration larger gains were obtained by the terminal fairings than by boattailing. The results also indicate some possible improvements in performance by careful nozzle-slot design.

Langley Research Center,
National Aeronautics and Space Administration,
Langley Field, Va., March 27, 1961.

REFERENCES

1. Swihart, John M., and Nelson, William J.: Performance of Multiple Jet-Exit Installations. NACA RM L58E01, 1958.

2. Swihart, John M., and Keith, Arvid L., Jr.: An Investigation of Clustered Jet-Exit Arrangements at Supersonic Speeds. NASA MEMO 5-11-59L, 1959.

3. Runckel, Jack F.: Preliminary Transonic Performance Results for Solid and Slotted Turbojet Nacelle Afterbodies Incorporating Fixed Divergent Jet Nozzles Designed for Supersonic Operation. NASA MEMO 10-24-58L, 1958.

4. Swihart, John M., Norton, Harry T., Jr., and Schmeer, James W.: Effect of Several Afterbody Modifications Including Terminal Fairings on the Drag of a Single-Engine Fighter Model With Hot-Jet Exhaust. NASA MEMO 10-29-58L, 1958.

5. Love, Eugene S., Grigsby, Carl E., Lee, Louise P., and Woodling, Mildred J.: Experimental and Theoretical Studies of Axisymmetric Free Jets. NASA TR R-6, 1959.

TABLE I

CONFIGURATION NOZZLE GEOMETRY

Configuration	β	θ	d_p	$\frac{d_e}{d_p}$	$\frac{l}{d_p}$	$\frac{d_b}{d_e}$	$\frac{d_e}{d_{max}}$	Design $p_{t,j}/p_\infty$	
								Cold air $\gamma = 1.4$	Hot exhaust $\gamma = 1.27$
5	6.86	16.62	0.300	1.78	1.84	1.00	0.80	22.9	18.8
8	0	6.24	.412	1.29	1.34	1.25	.80	7.7	6.6
9	0	12.00	.356	1.87	2.05	1.00	1.00	27.1	22.0

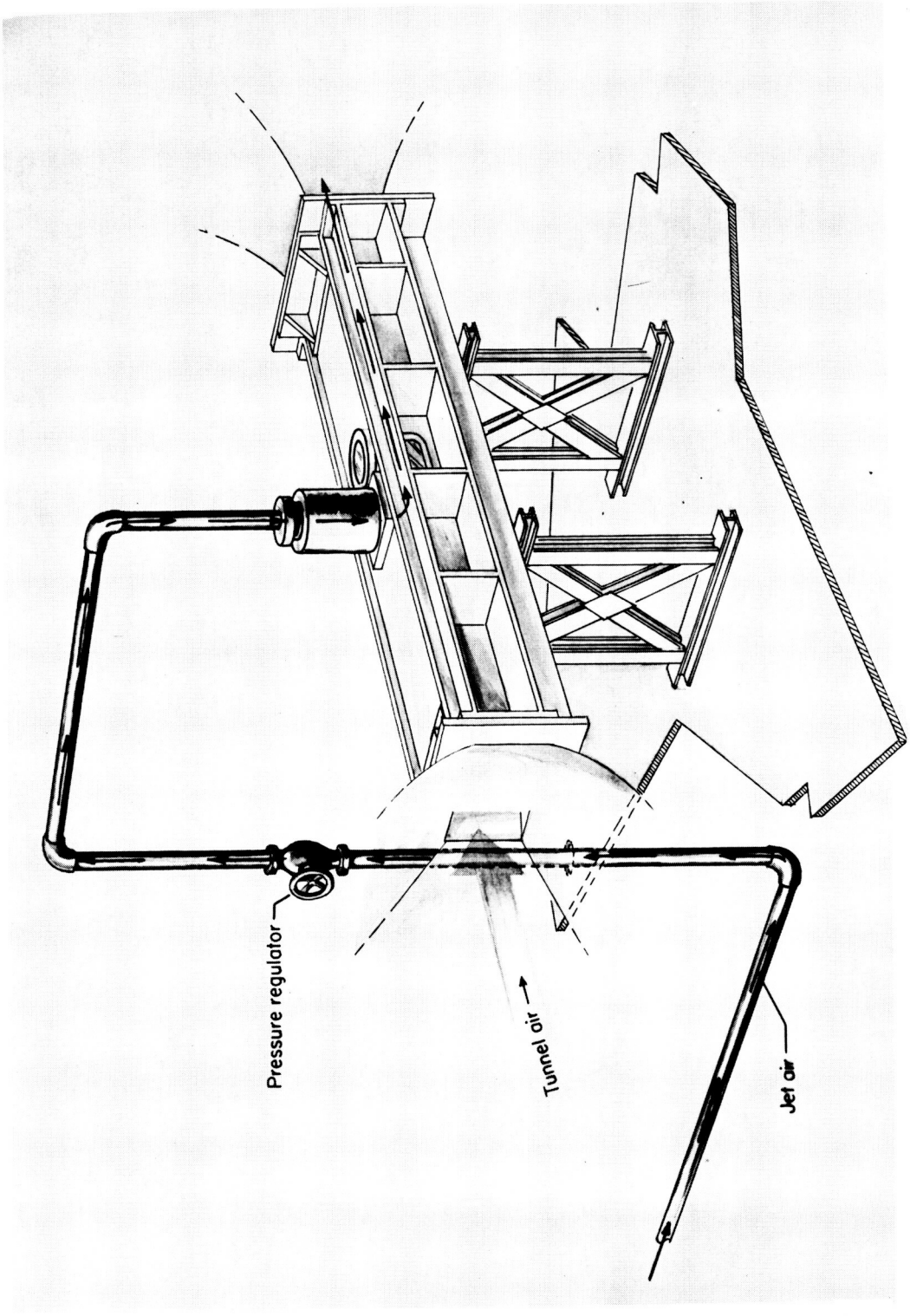

(a) Jet air supply piping and general view of tunnel.

Figure 1.- General test arrangement.

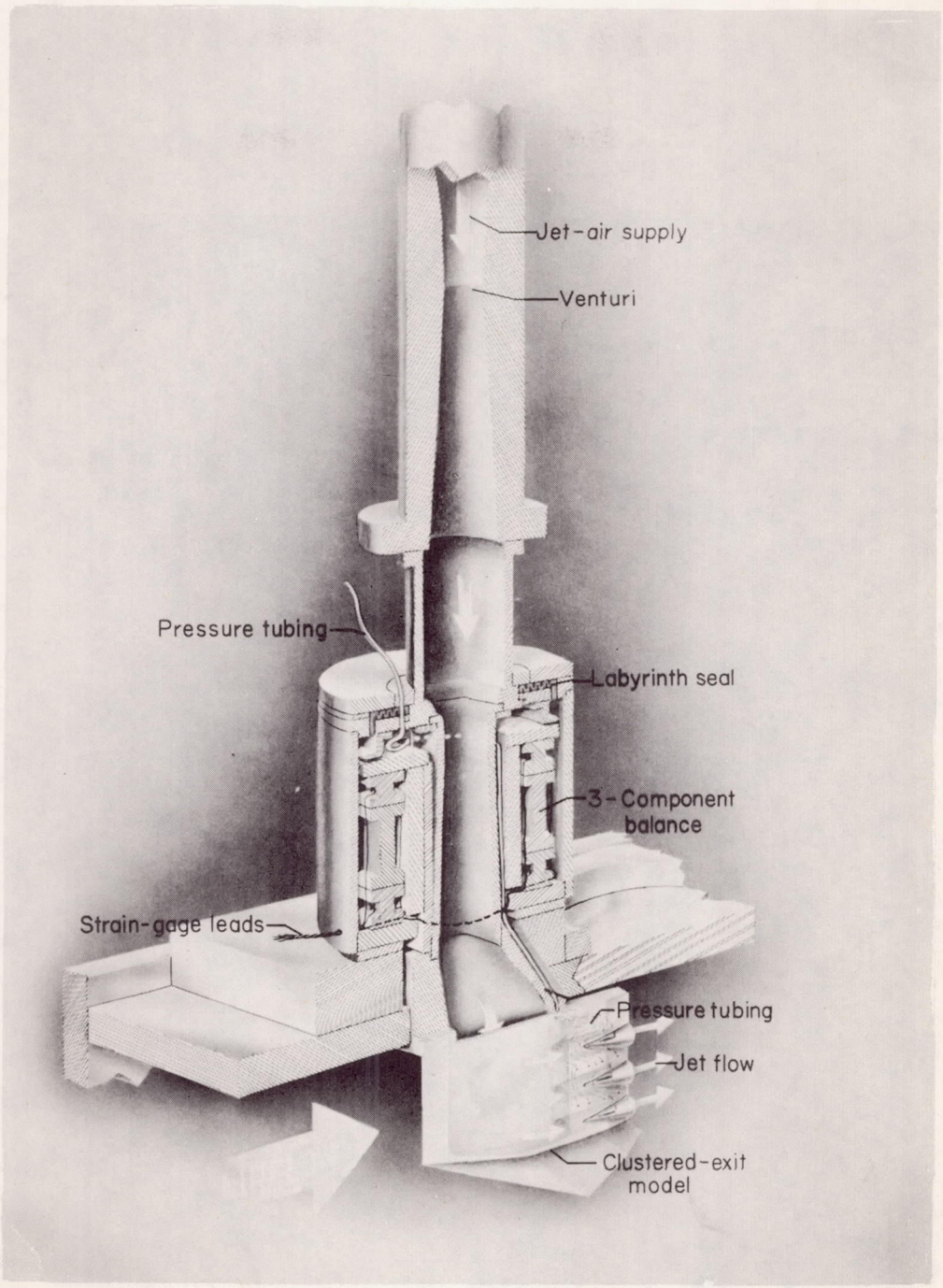

(b) Model installation.

Figure 1.- Concluded.

(a) Configuration 9 installed. L-58-3780.1

Figure 2.- Photographs of the complete model.

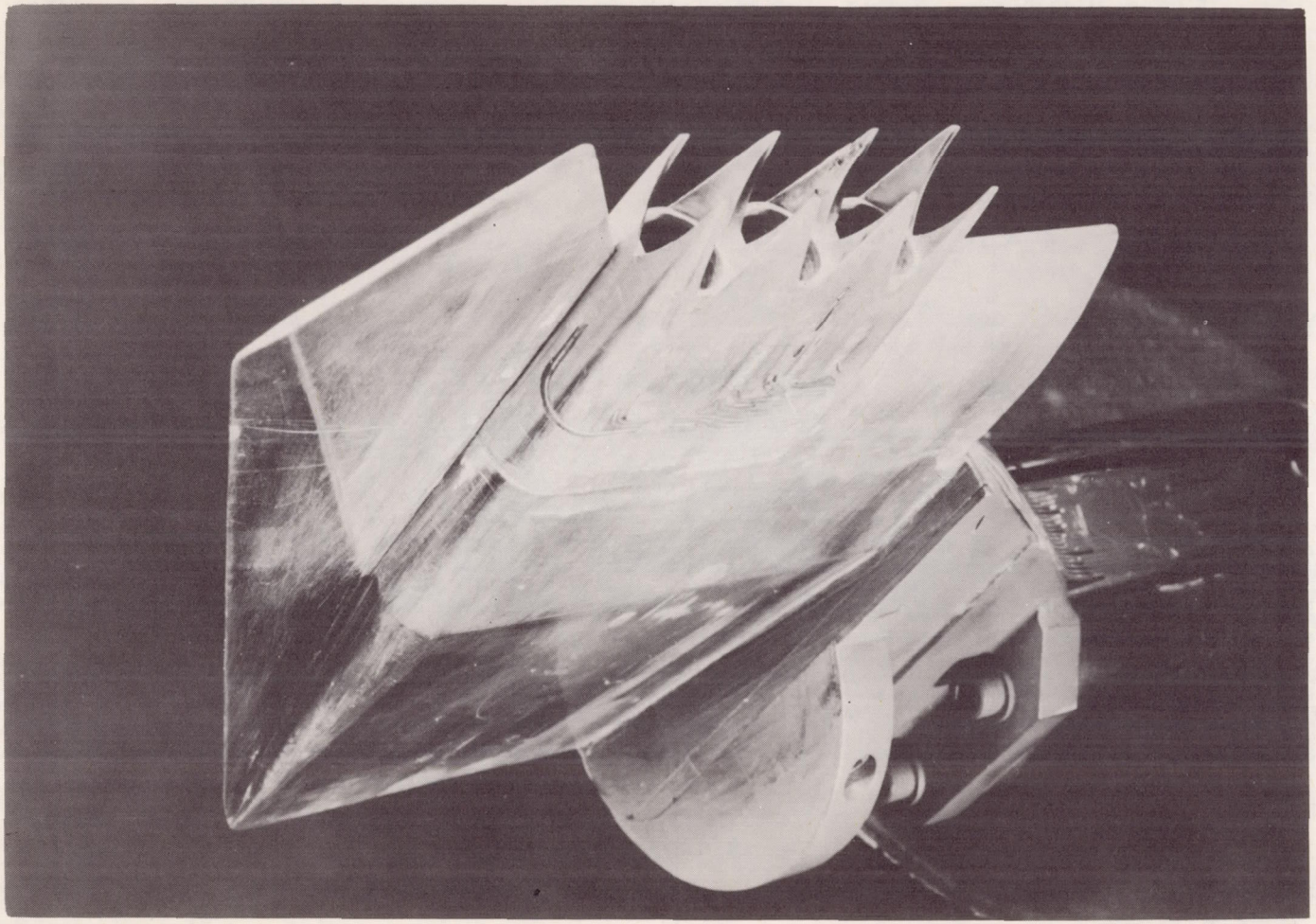

(b) Configuration 8 with terminal fairing. L-58-27

Figure 2.- Concluded.

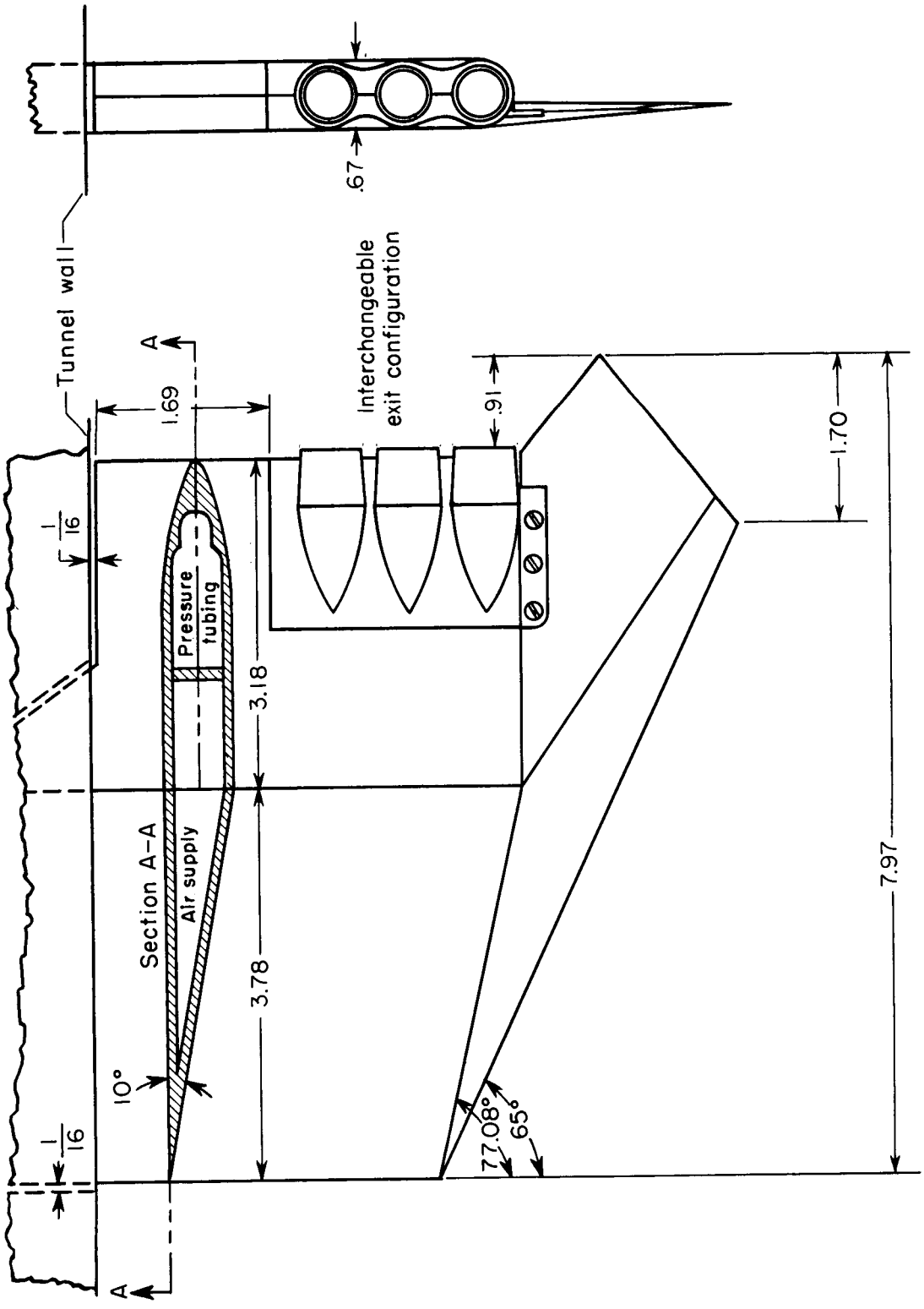

Figure 3.- Geometric details of clustered exit model. All dimensions in inches.

L-1293

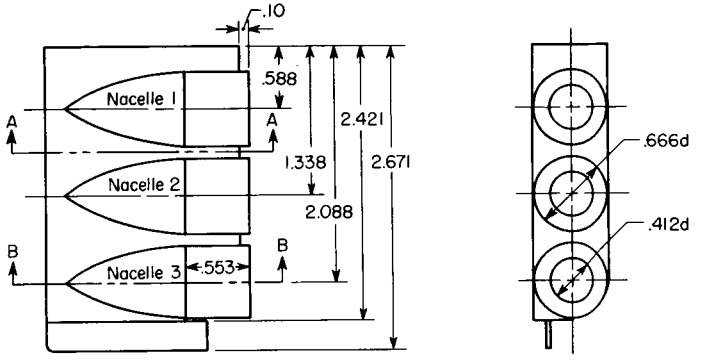

Configuration 5

PRESSURE ORIFICE LOCATIONS
Configuration 5

Wing upper and lower surface between nacelles 2 and 3

x	x/d_p
0.00	0.000
−.25	−.607
−.50	−1.215
−.75	−1.821
−1.00	−2.426
−1.25	−3.032

Note: A pressure orifice is also located at x = 0 between nacelles 1 and 2.

ORDINATES FOR FAIRING BETWEEN NACELLES

Configuration 5	
x	y
0.00	0.000
−.16	.104
−.32	.106
−.48	.208
−.64	.248
−.80	.280
−.96	.303
−1.12	.320
−1.28	.328
−1.44	.333

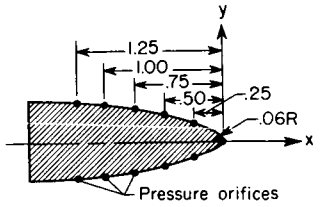

Section A–A

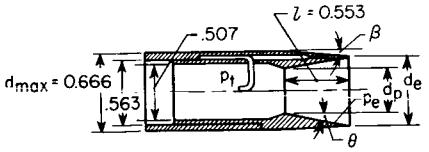

Section B–B

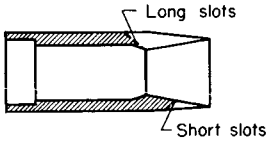

Section B–B, long and short slots

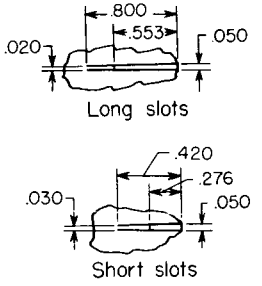

(a) Nozzle geometry and pressure orifice locations.

Figure 4.- Details of interchangeable exit configurations.

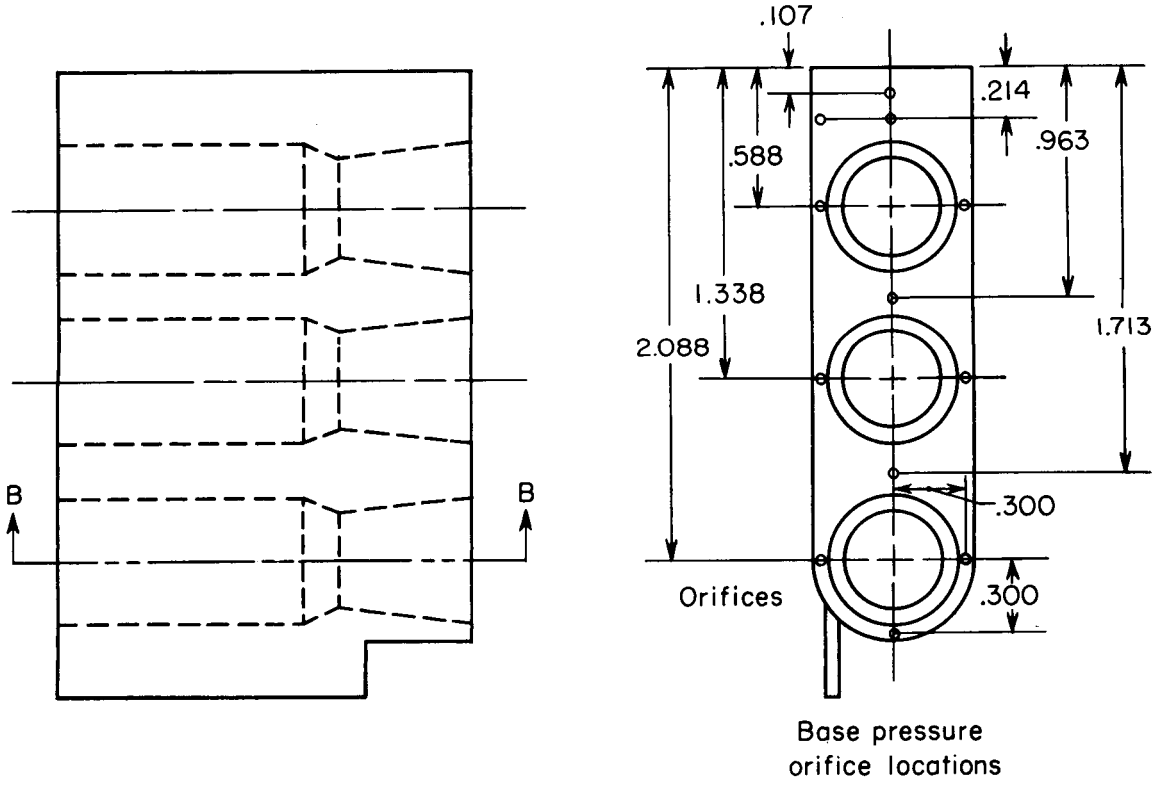

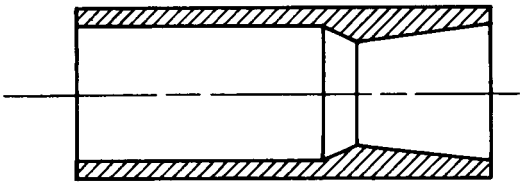

(b) Configuration 8.

Figure 4.- Continued.

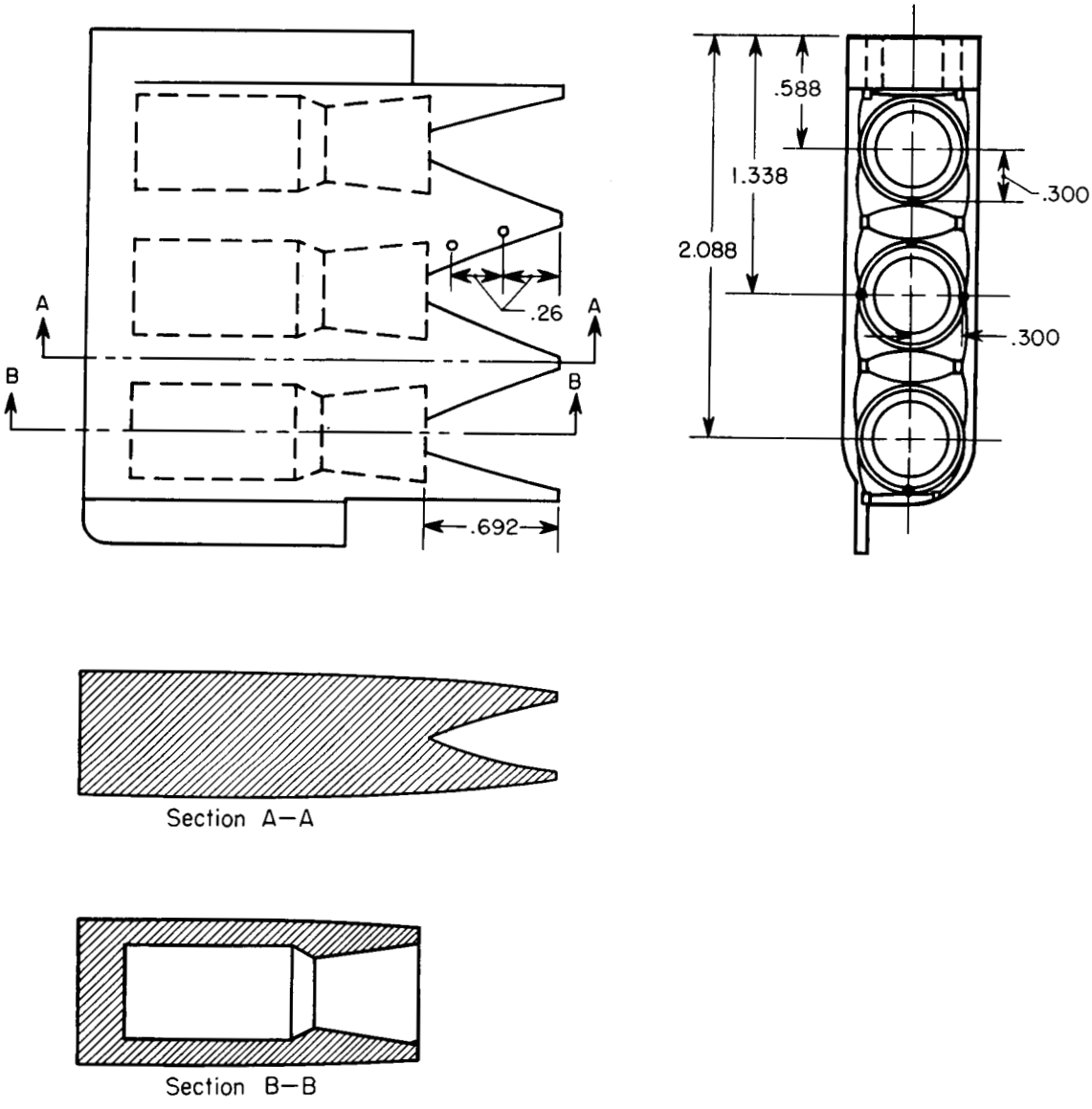

(c) Configuration 8 with terminal fairings.

Figure 4.- Continued.

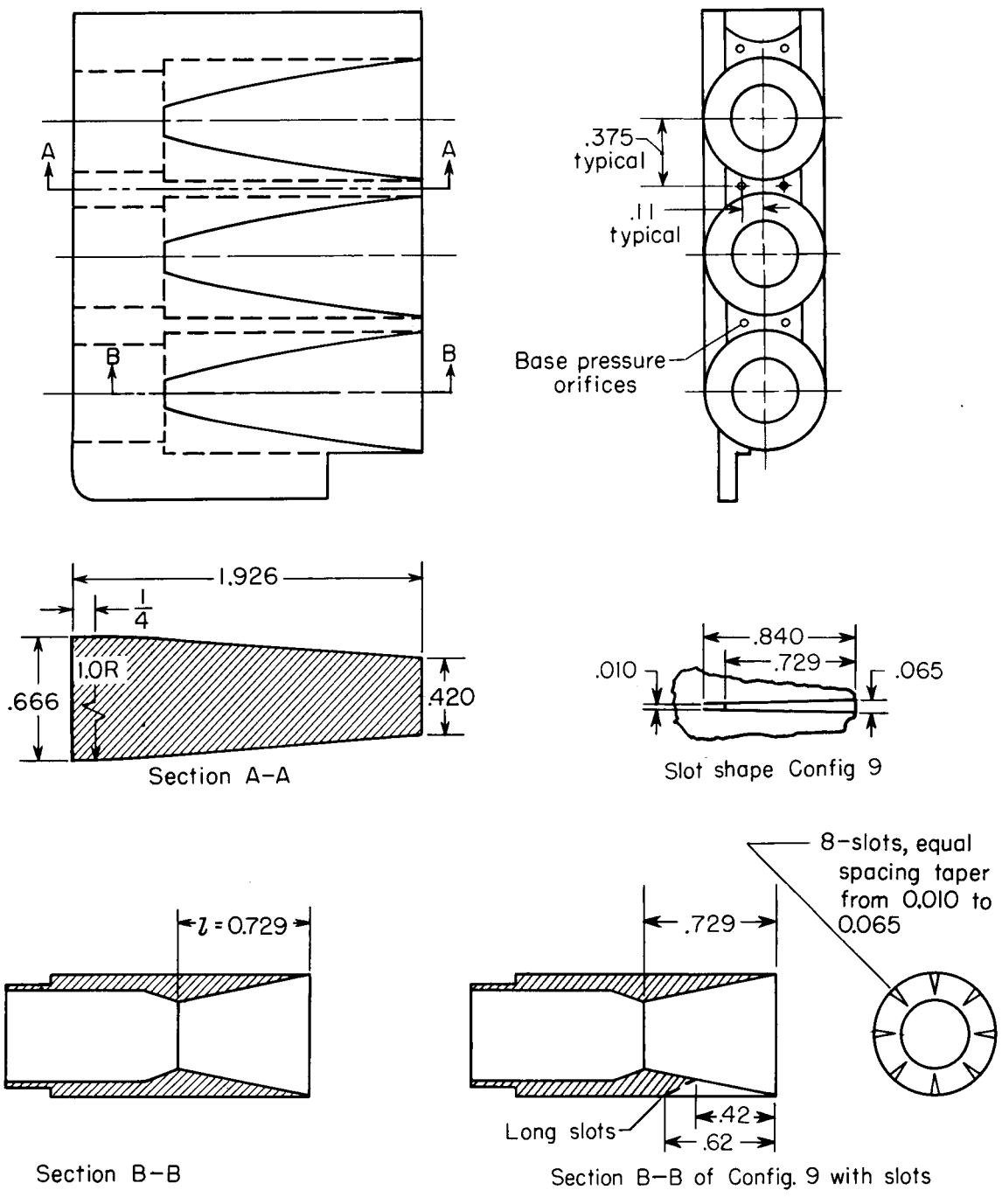

(d) Configuration 9.

Figure 4.- Concluded.

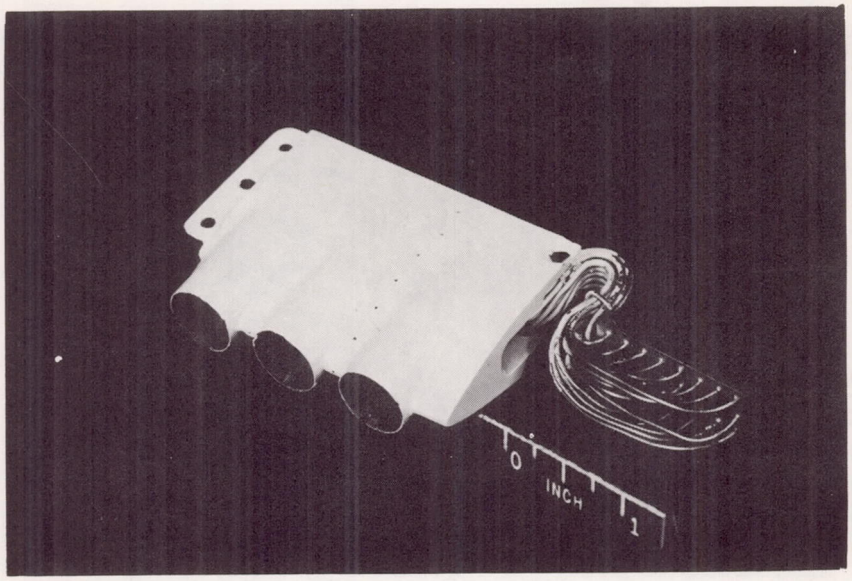

Configuration 5 L-59-4416

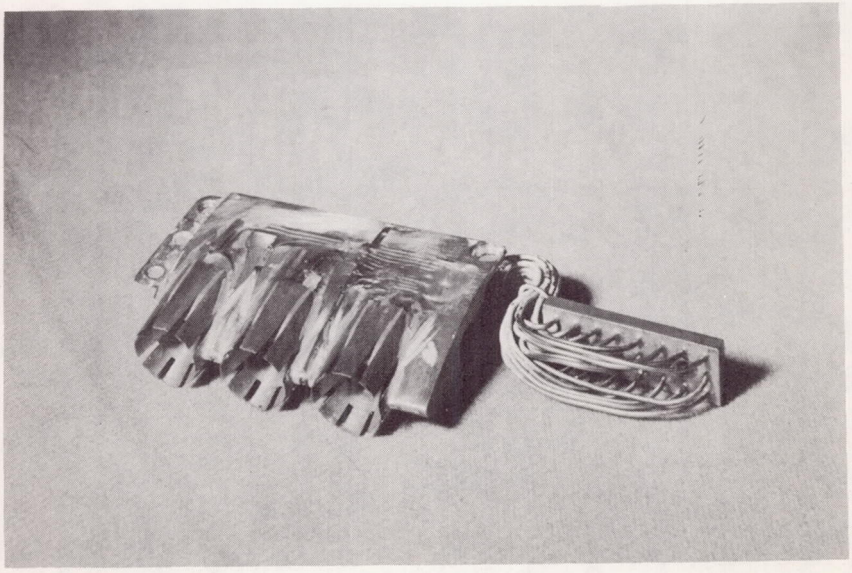

Configuration 5, short slots

L-59-1330

(a) Configuration 5 and configuration 5 with short slots.

Figure 5.- Photographs of the clustered exits.

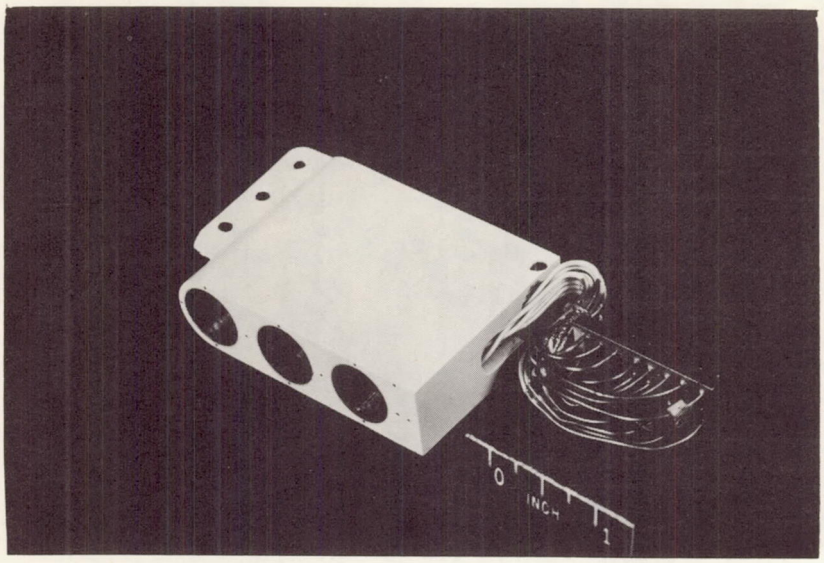

Configuration 8 L-59-4417

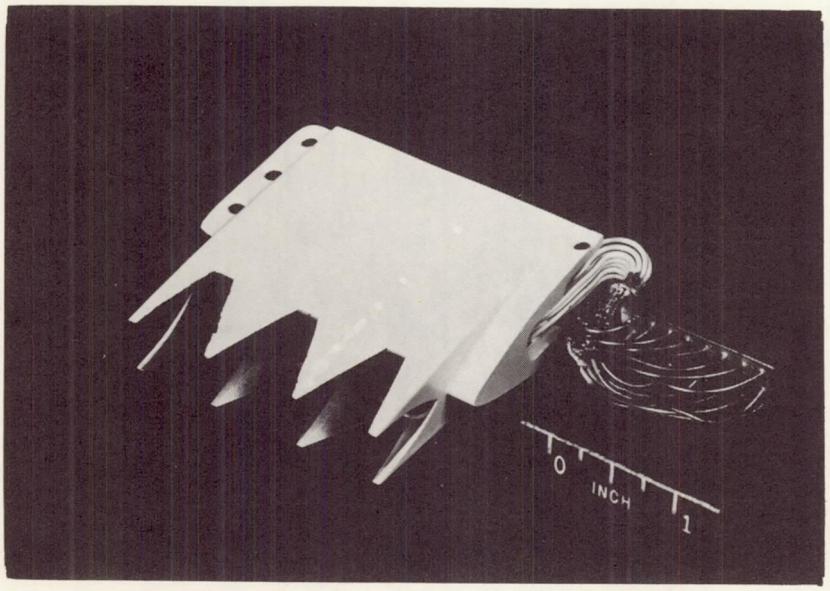

Configuration 8, terminal fairings

L-59-4413

(b) Configuration 8 and configuration 8 with terminal fairings.

Figure 5.- Continued.

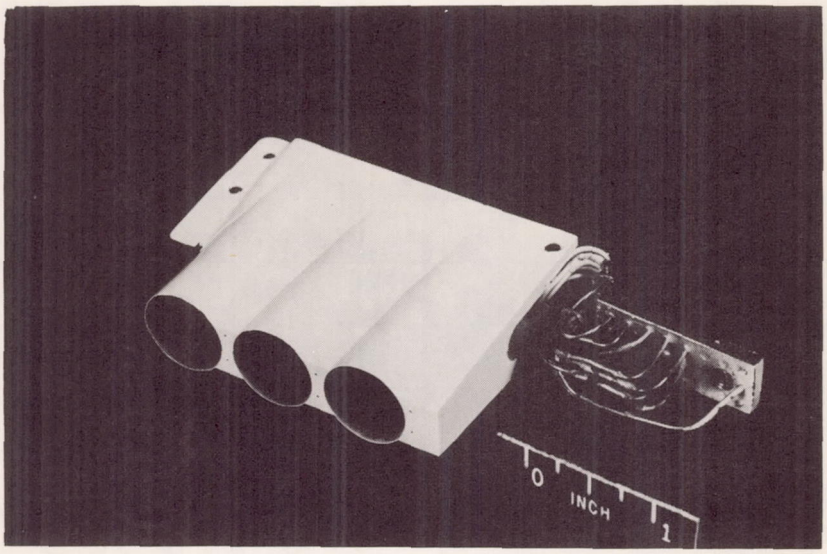

Configuration 9 L-59-4412

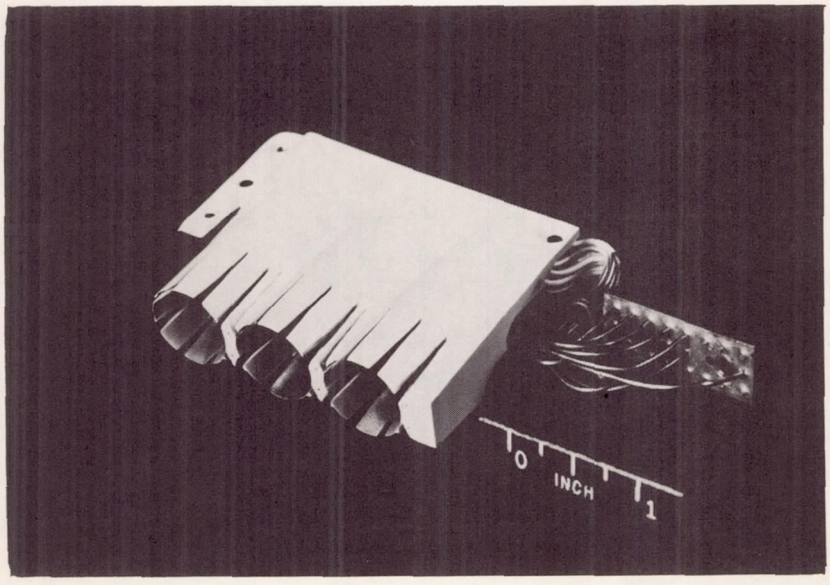

Configuration 9, slotted

L-59-4414

(c) Configuration 9 and configuration 9 with slots.

Figure 5.- Concluded.

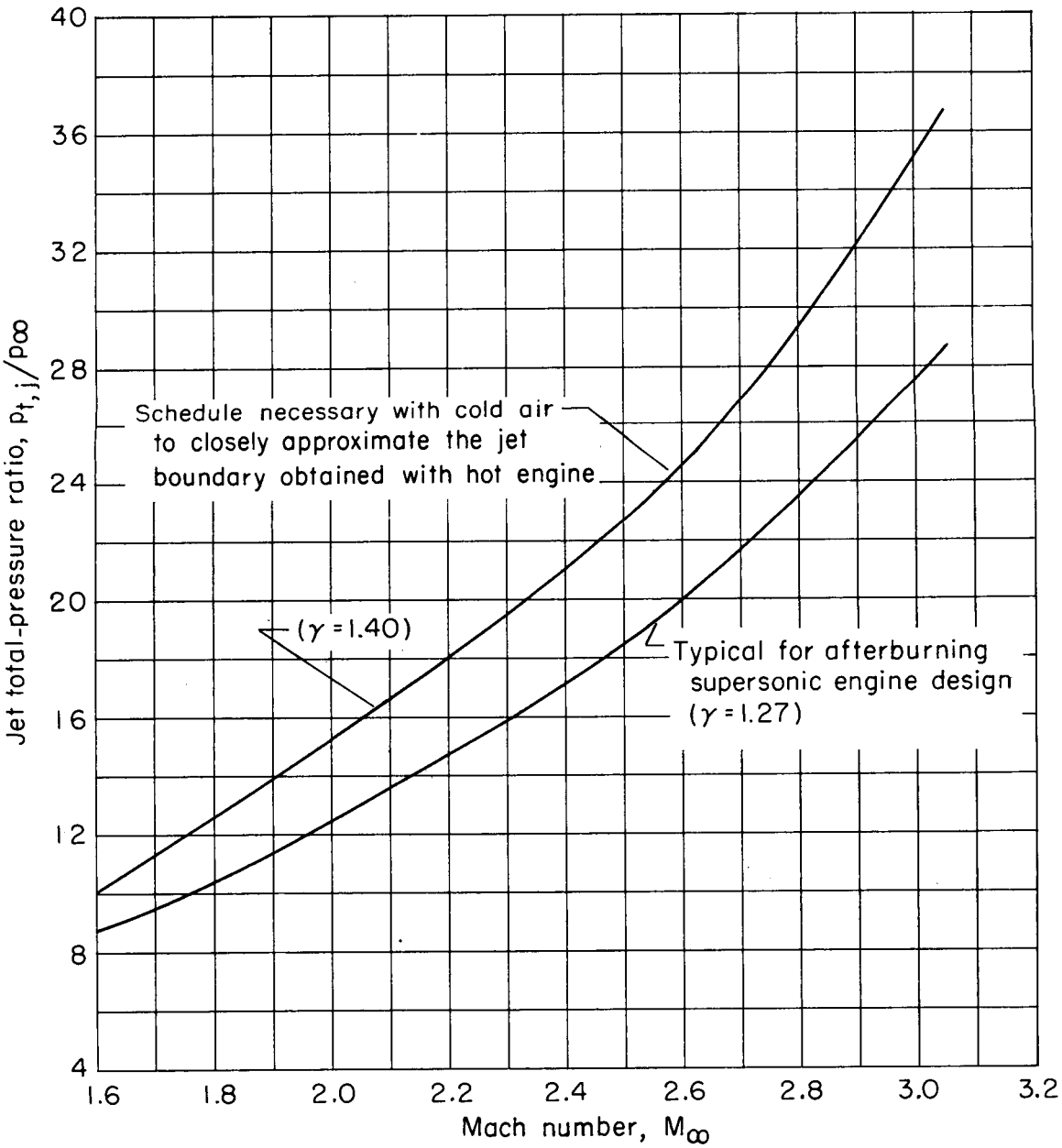

Figure 6.- Comparison between jet total-pressure ratio with Mach number for hot jet (γ = 1.27) and cold jet (γ = 1.4) which produce the same initial jet boundary slope.

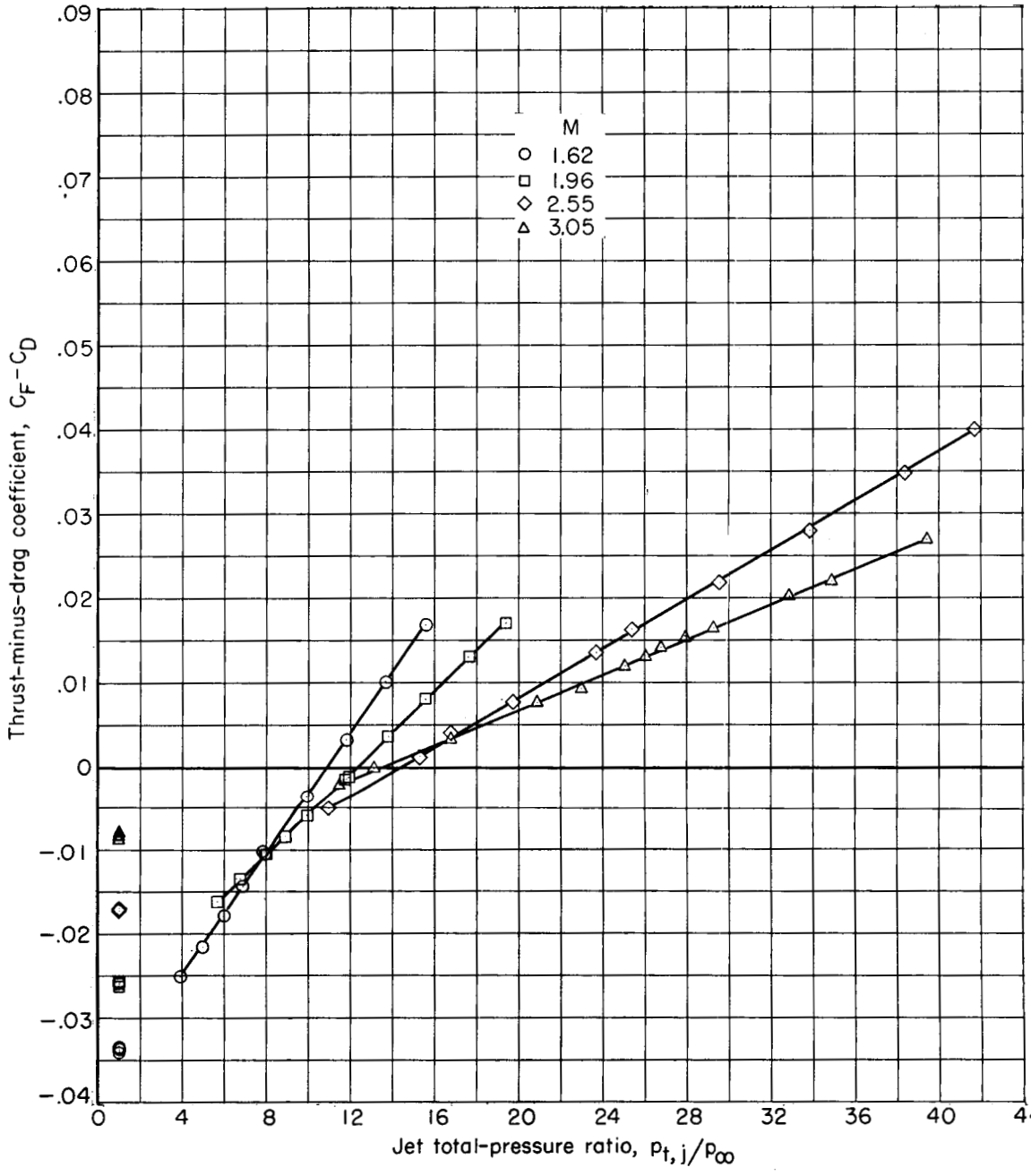

(a) Configuration 5.

Figure 7.- Effect of jet total-pressure ratio on measured thrust-minus-drag coefficient.

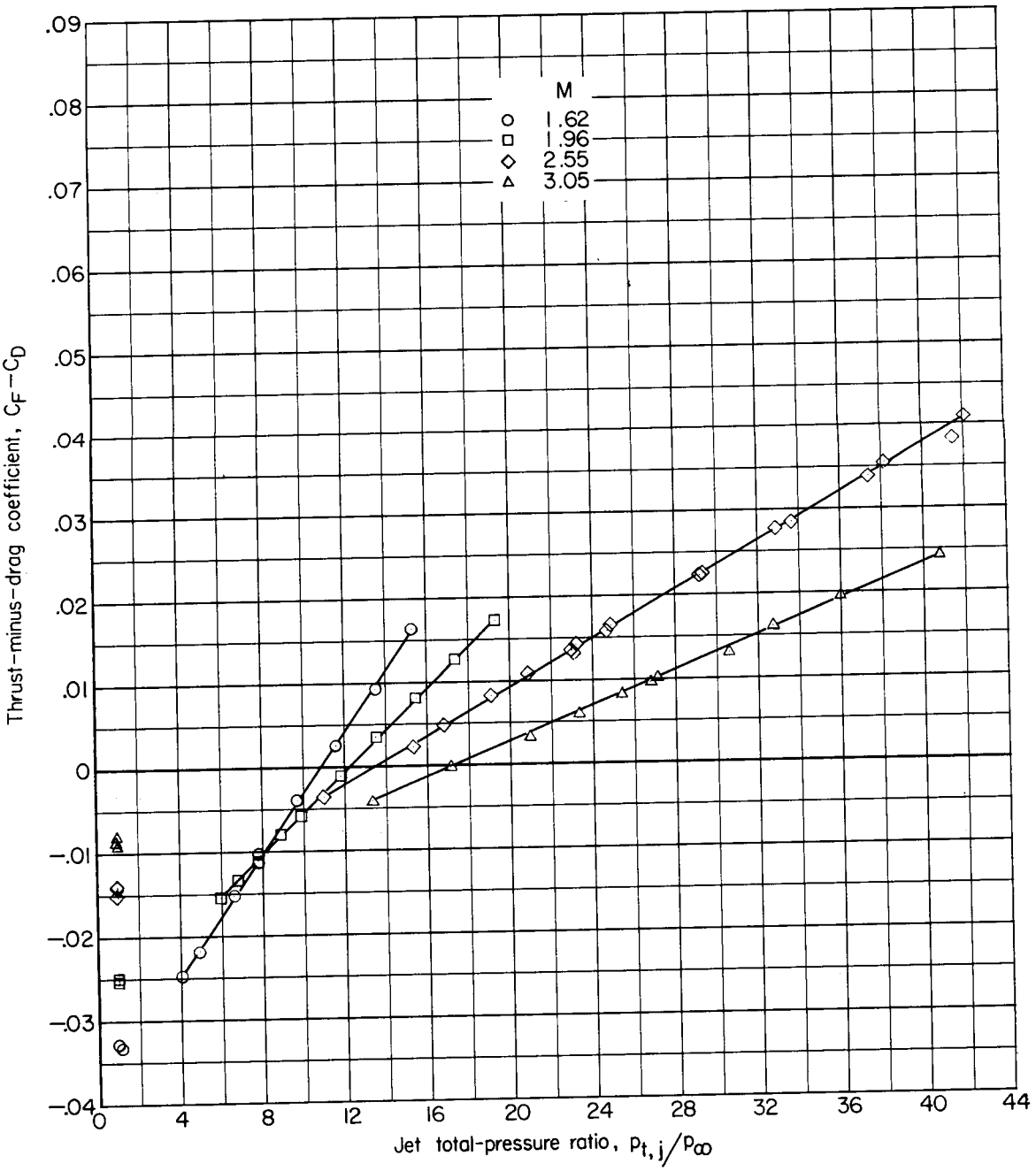

(b) Configuration 5 with short slots.

Figure 7.- Continued.

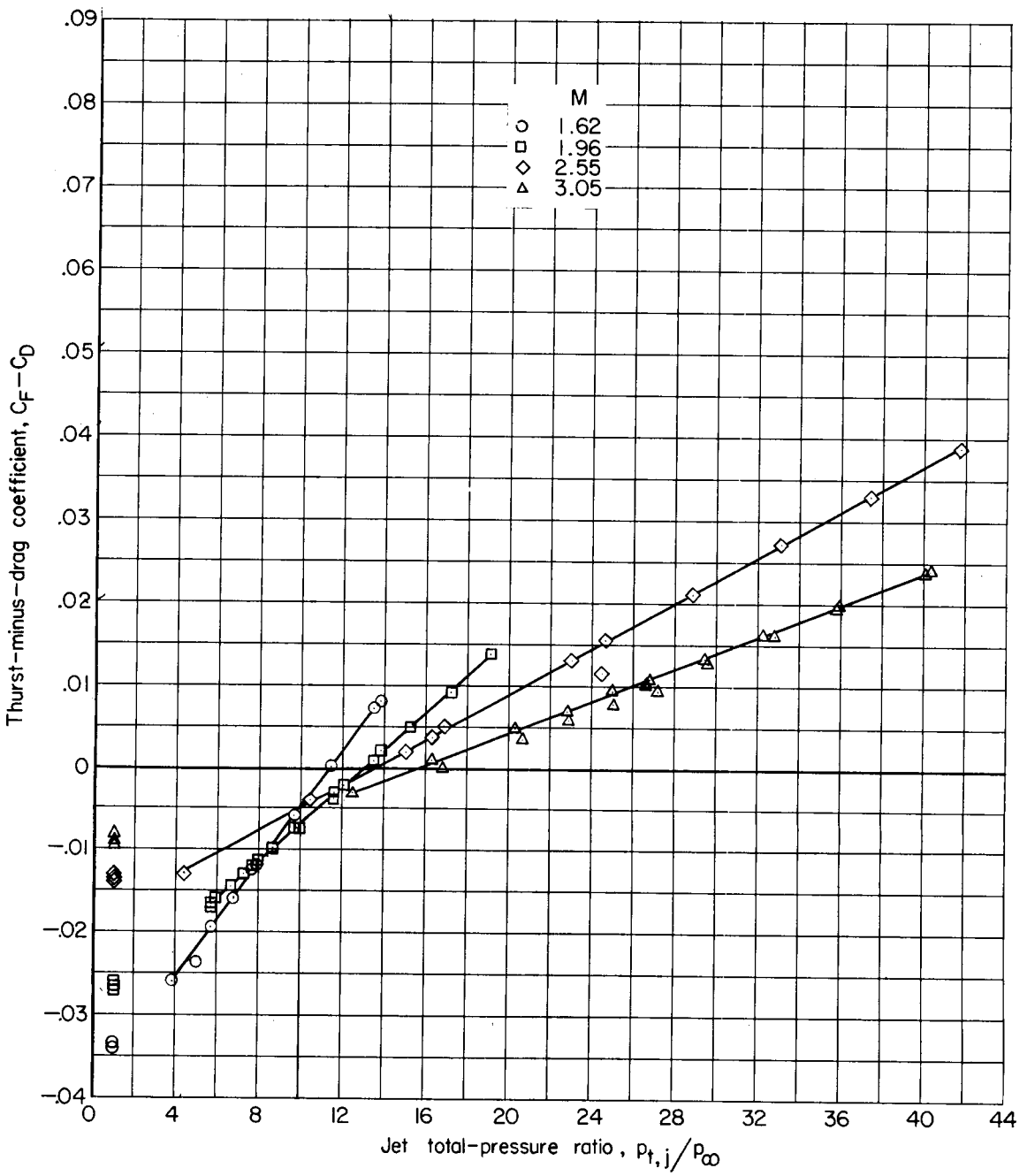

(c) Configuration 5 with long slots.

Figure 7.- Continued.

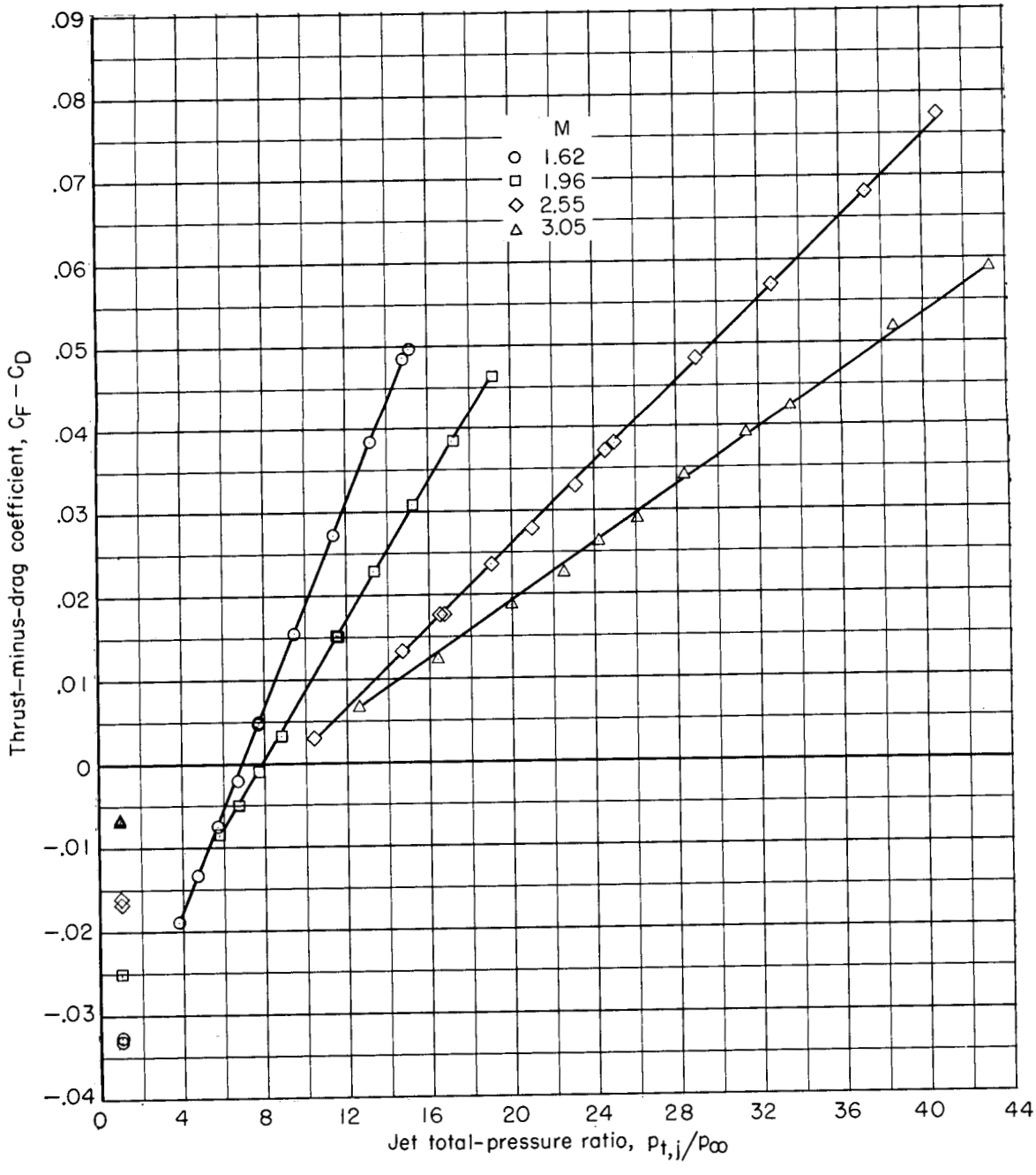

(d) Configuration 8.

Figure 7.- Continued.

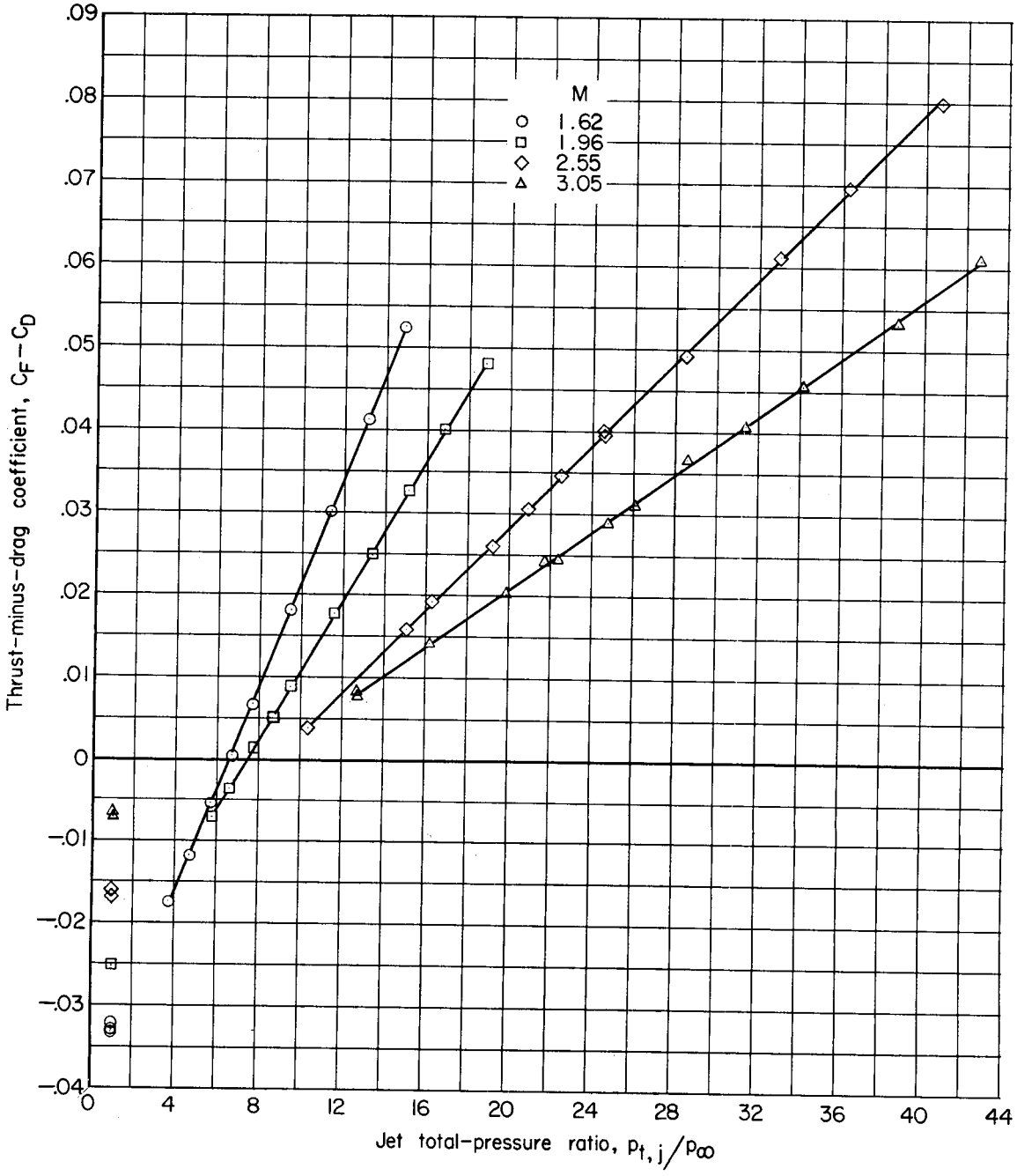

(e) Configuration 8 with terminal fairings.

Figure 7.- Continued.

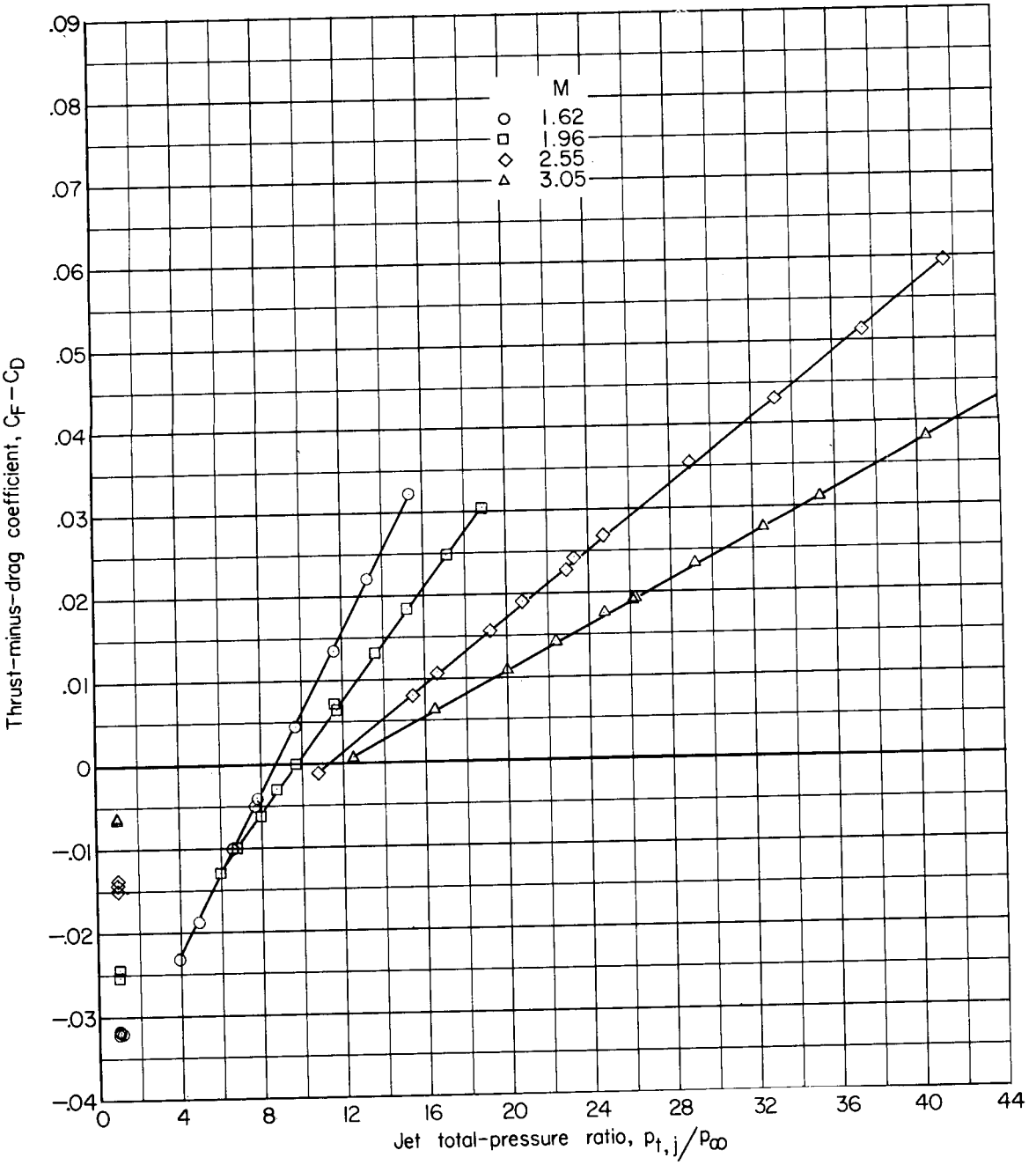

(f) Configuration 9.

Figure 7.- Continued.

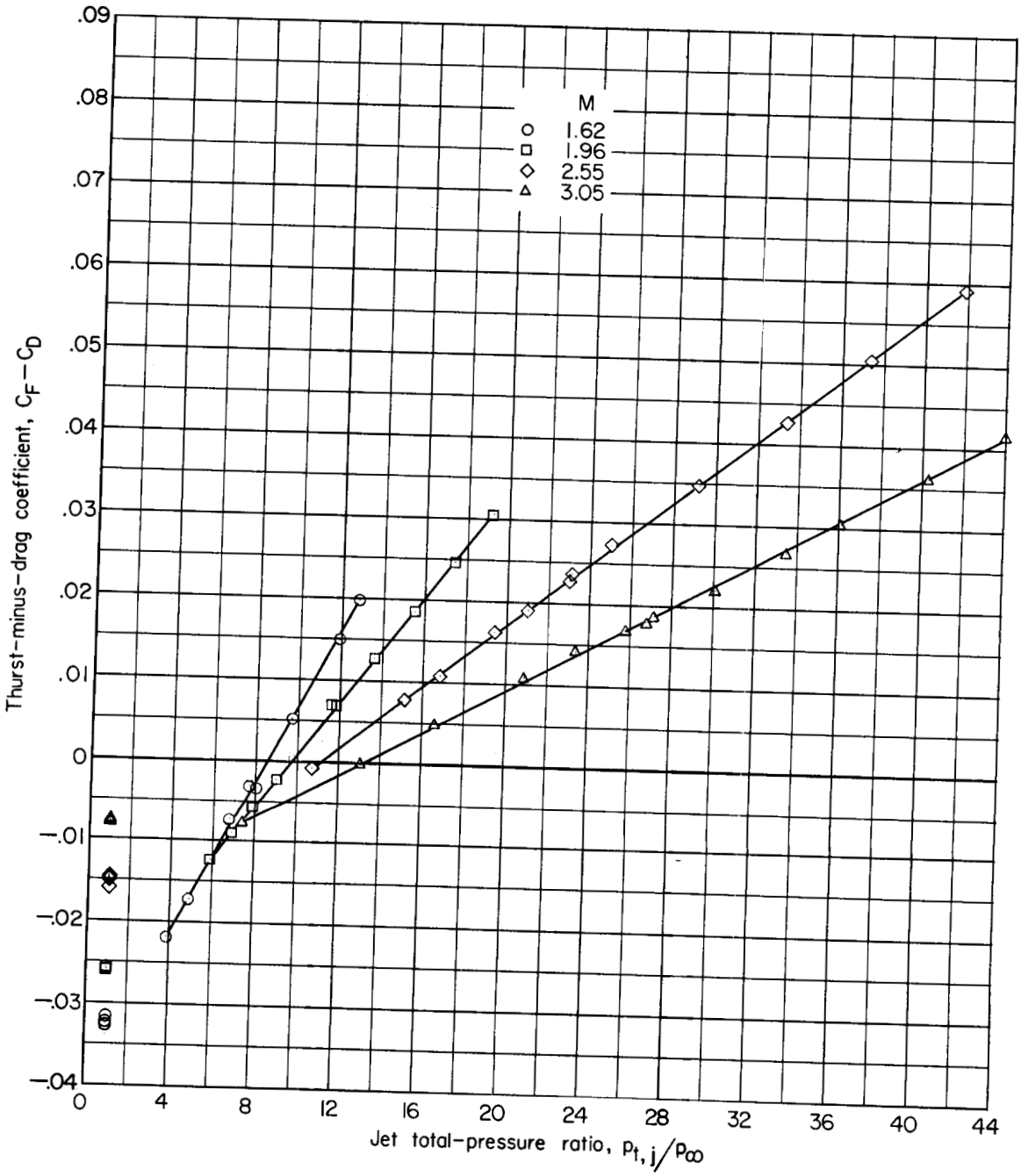

(g) Configuration 9 with slots.

Figure 7.- Concluded.

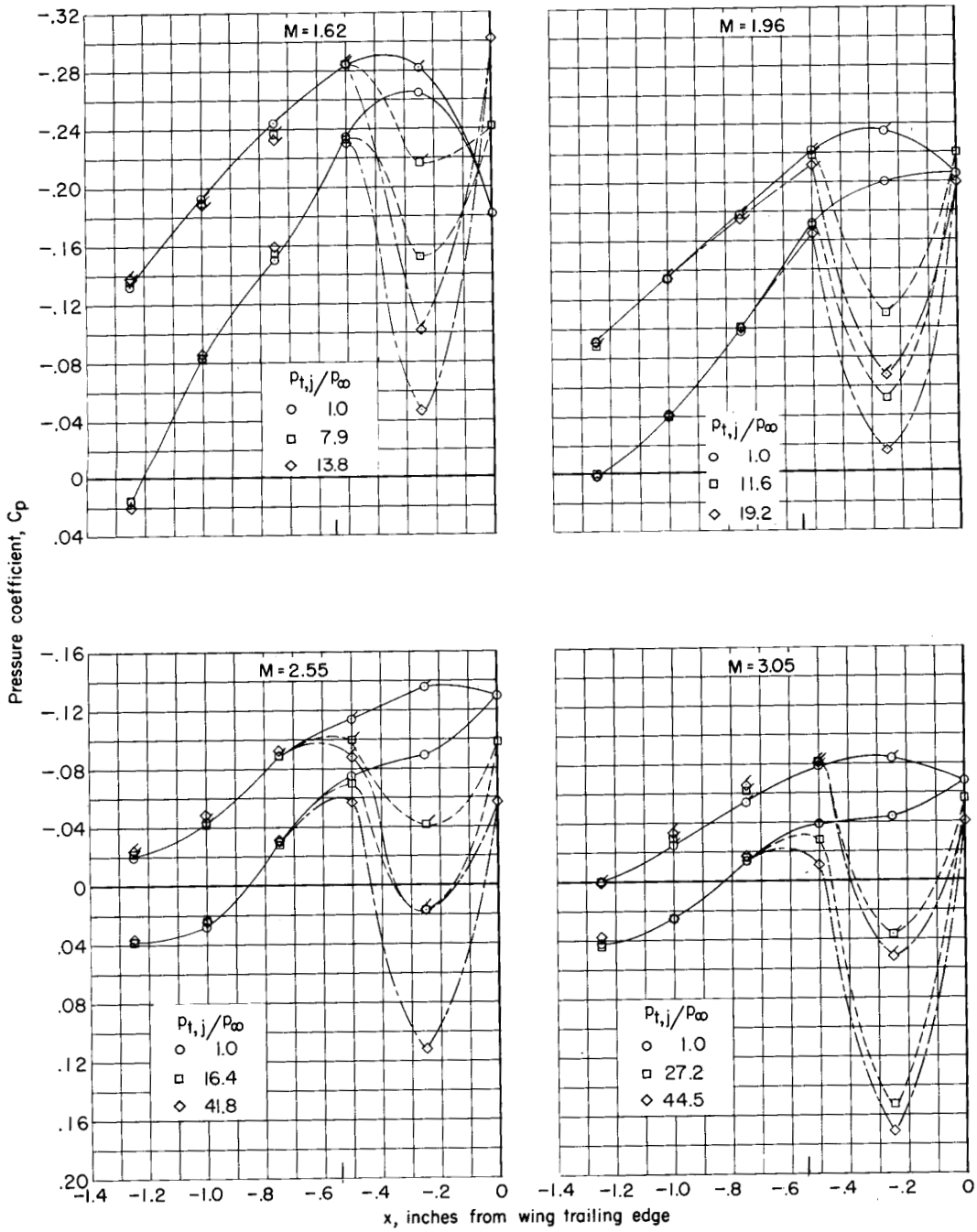

Figure 8.- Variation of pressure coefficient with distance from wing trailing edge along fairing between nacelles on configuration 5 with long slots. Flagged symbols are for lower surface. Ticks indicate throat position.

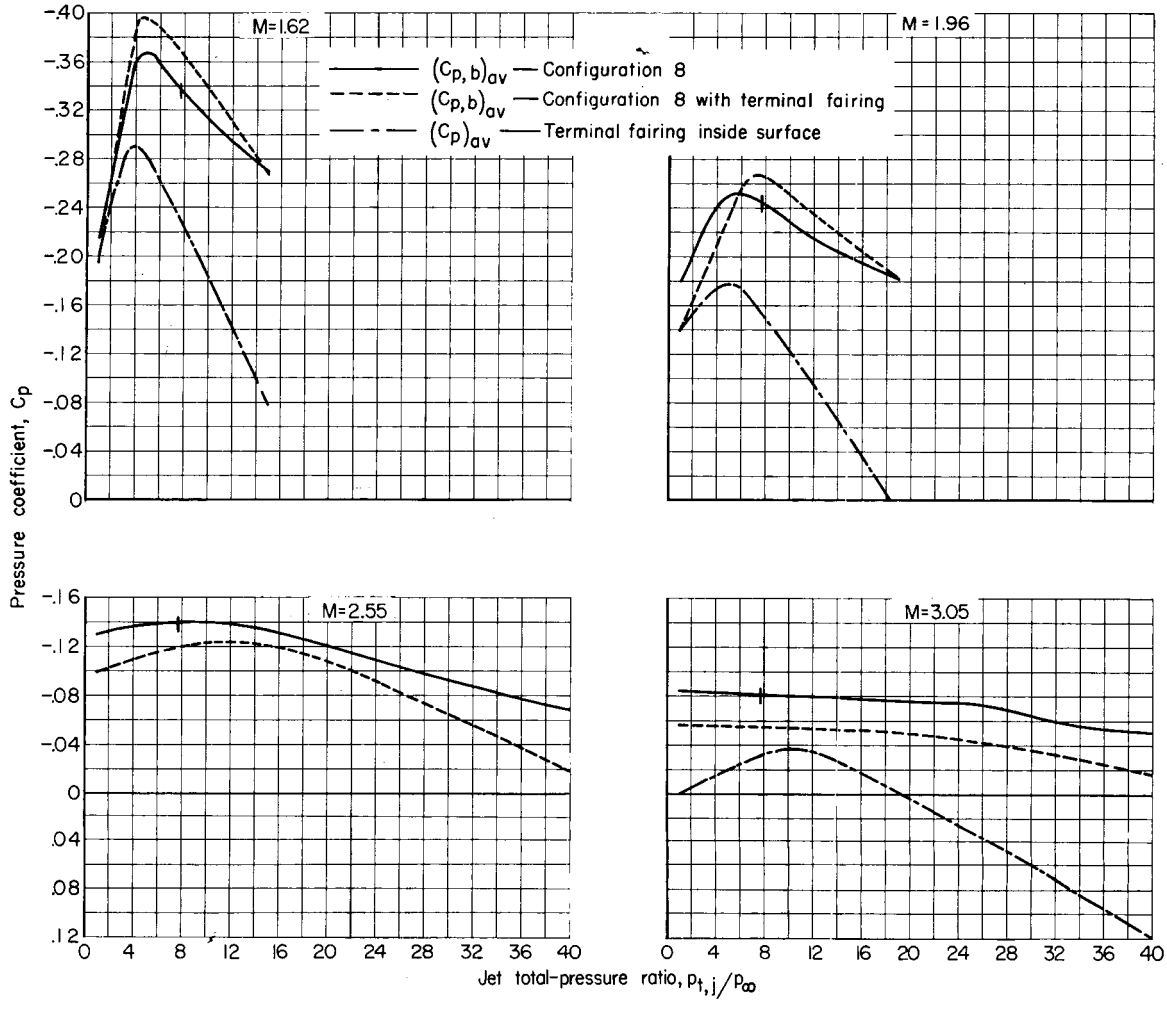

Figure 9.- Effect of jet total-pressure ratio on base pressure coefficients and terminal fairing surface pressure coefficients for configuration 8 at several Mach numbers. Ticks indicate design $p_{t,j}/p_\infty$ (cold air).

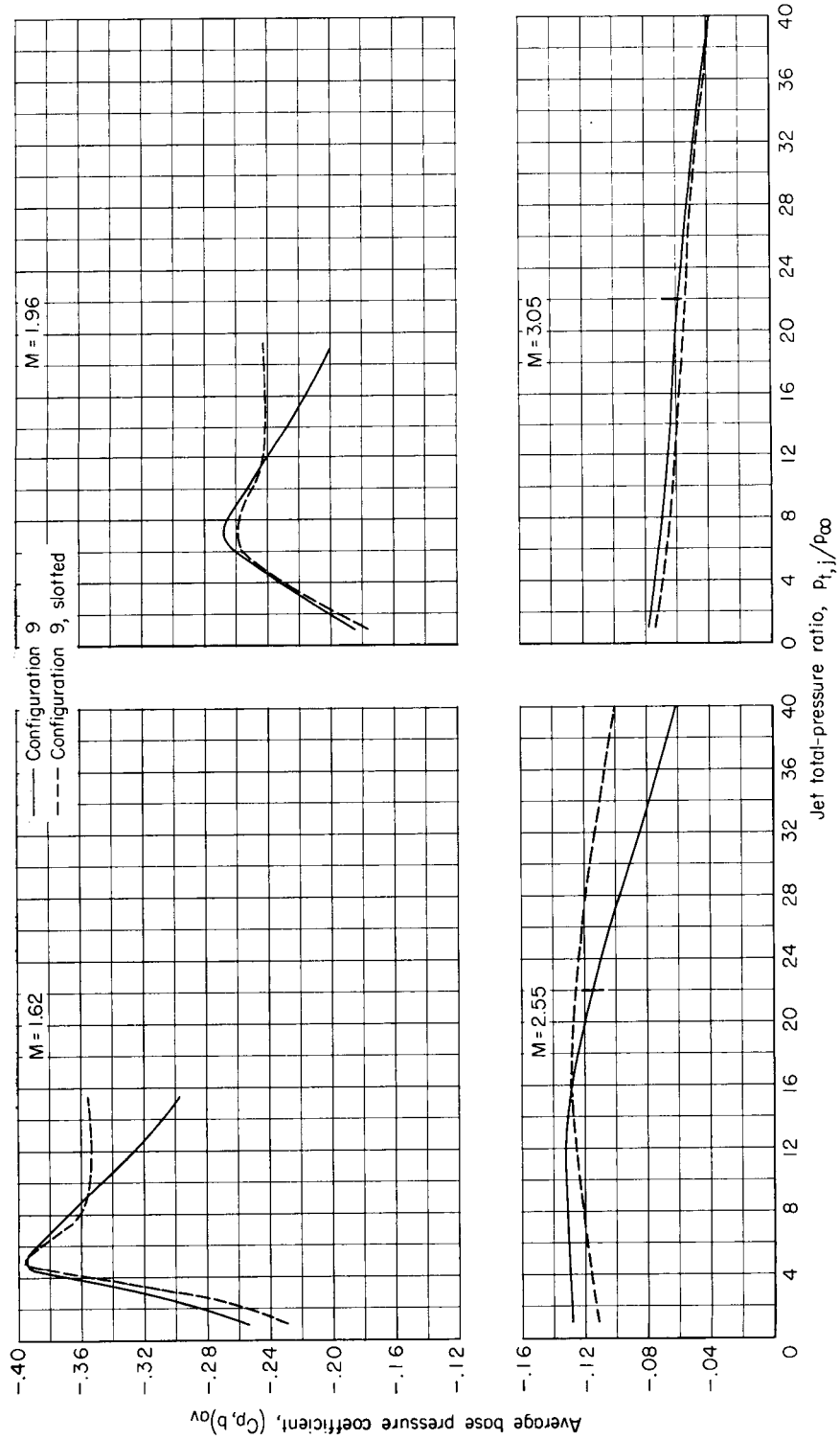

Figure 10.- Effect of jet total-pressure ratio on base pressure coefficients for configuration 9 at several Mach numbers. Ticks indicate design $p_{t,j}/p_\infty$ (cold air).

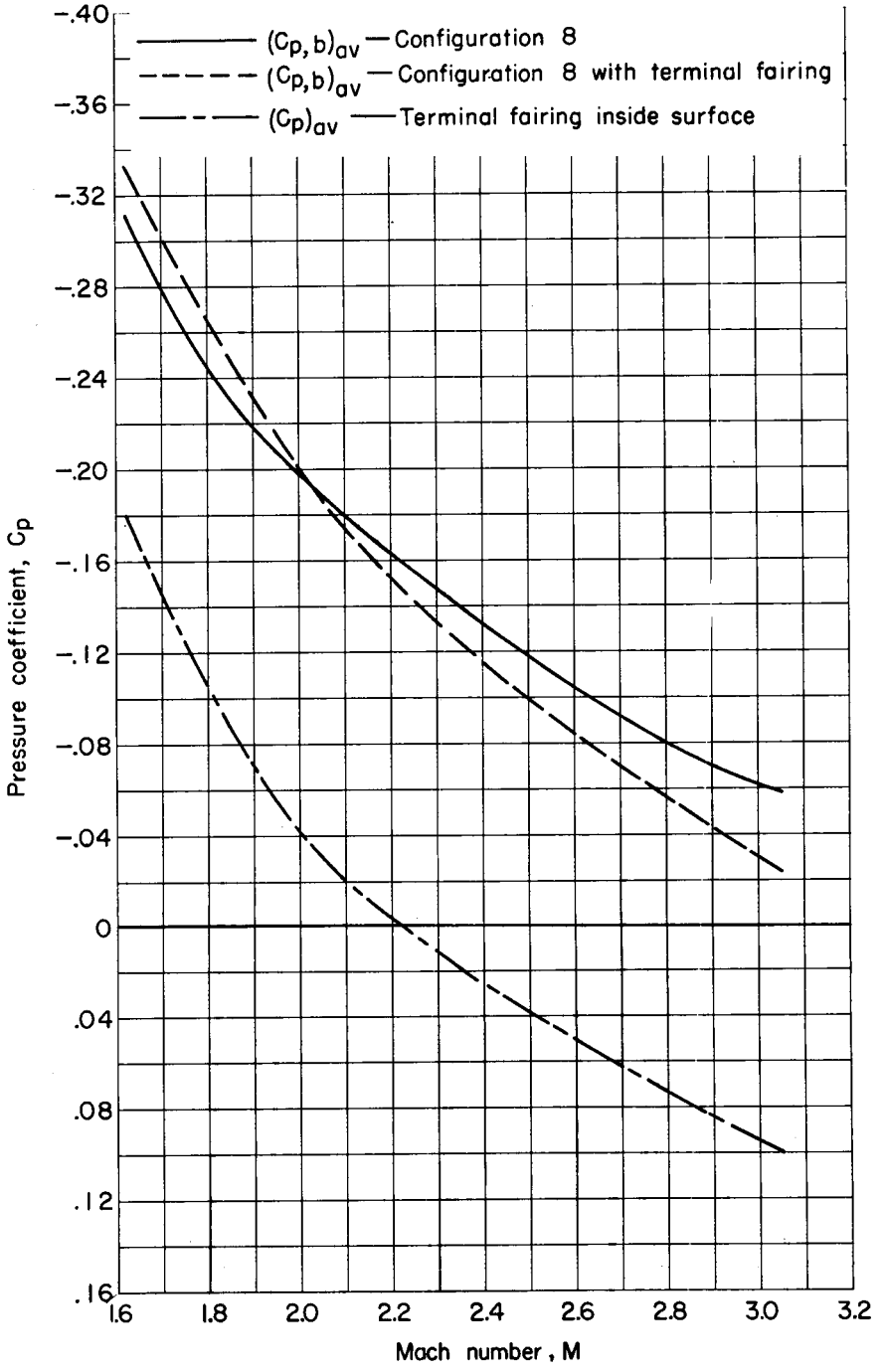

Figure 11.- Comparison of base and terminal fairing pressure coefficient for a schedule variation of jet total-pressure ratio. Configuration 8 and configuration 8 with terminal fairings.

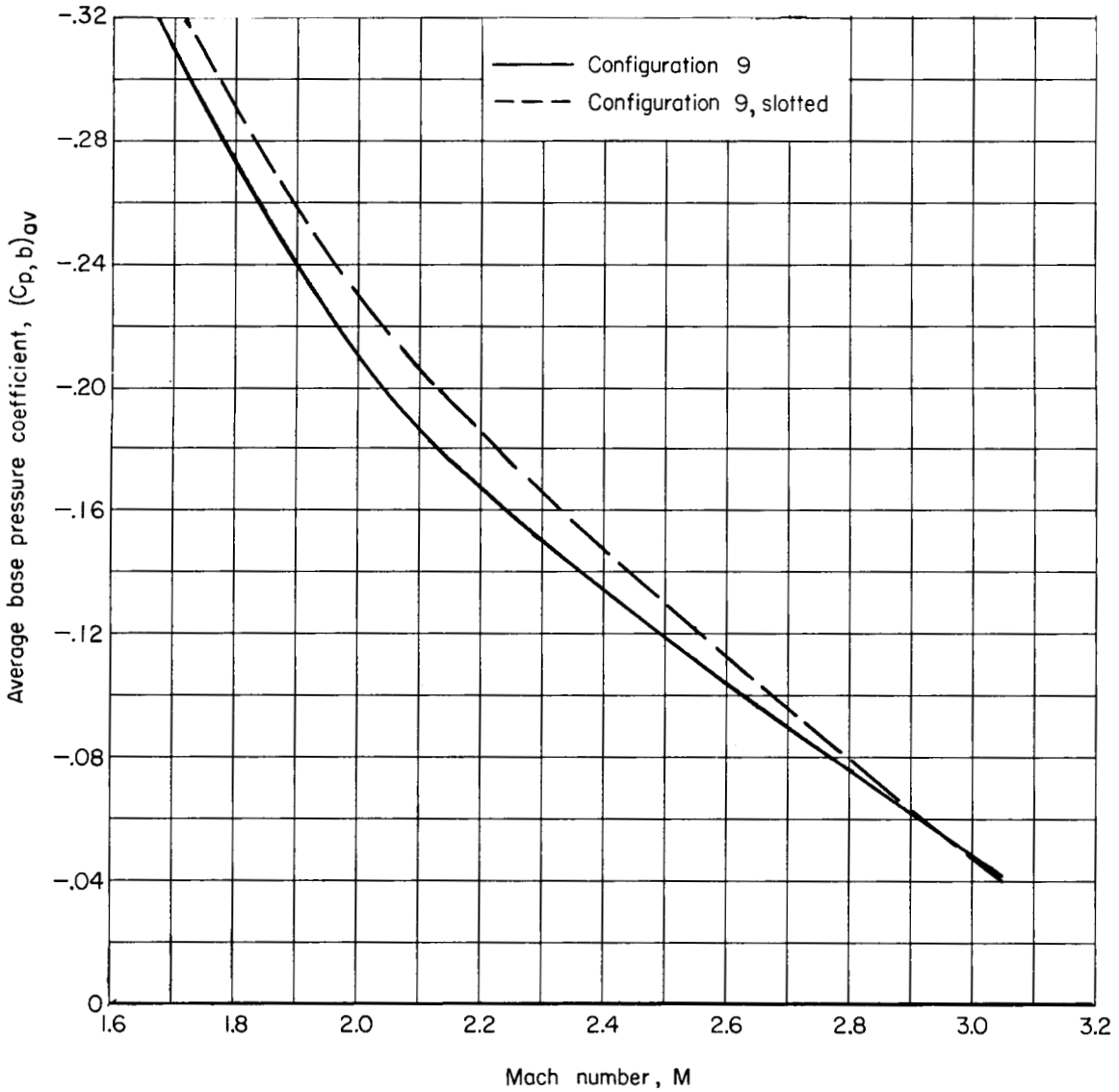

Figure 12.- Comparison of average base pressure coefficients for configuration 9 and configuration 9 slotted for scheduled variation of jet total-pressure ratio.

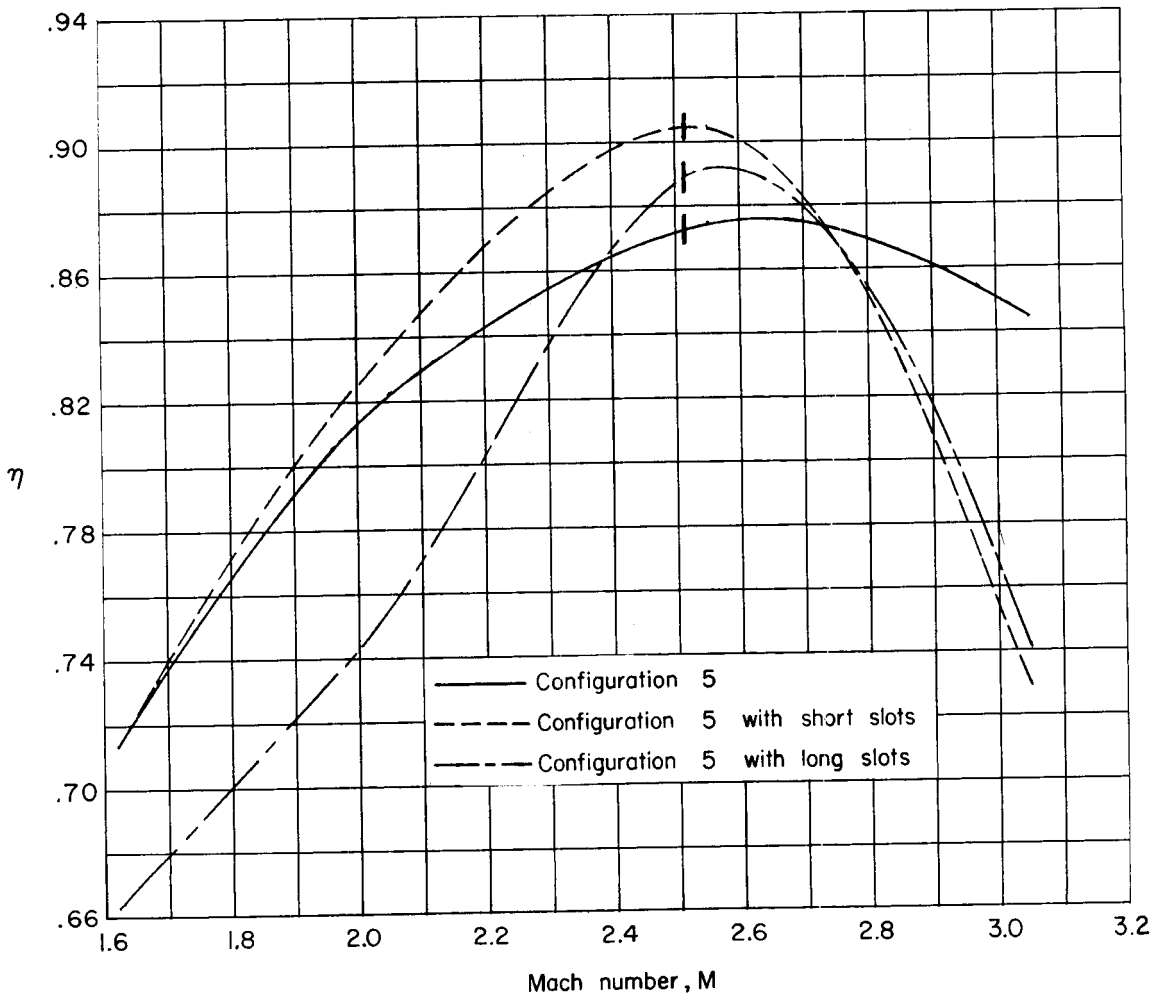

(a) Comparison of configuration 5, configuration 5 with short slots, and configuration 5 with long slots.

Figure 13.- Effect of Mach number on configuration efficiency factor. Data are for pressure ratio schedule for cold air shown in figure 6. Ticks indicate Mach number at which nozzle is on design pressure ratio.

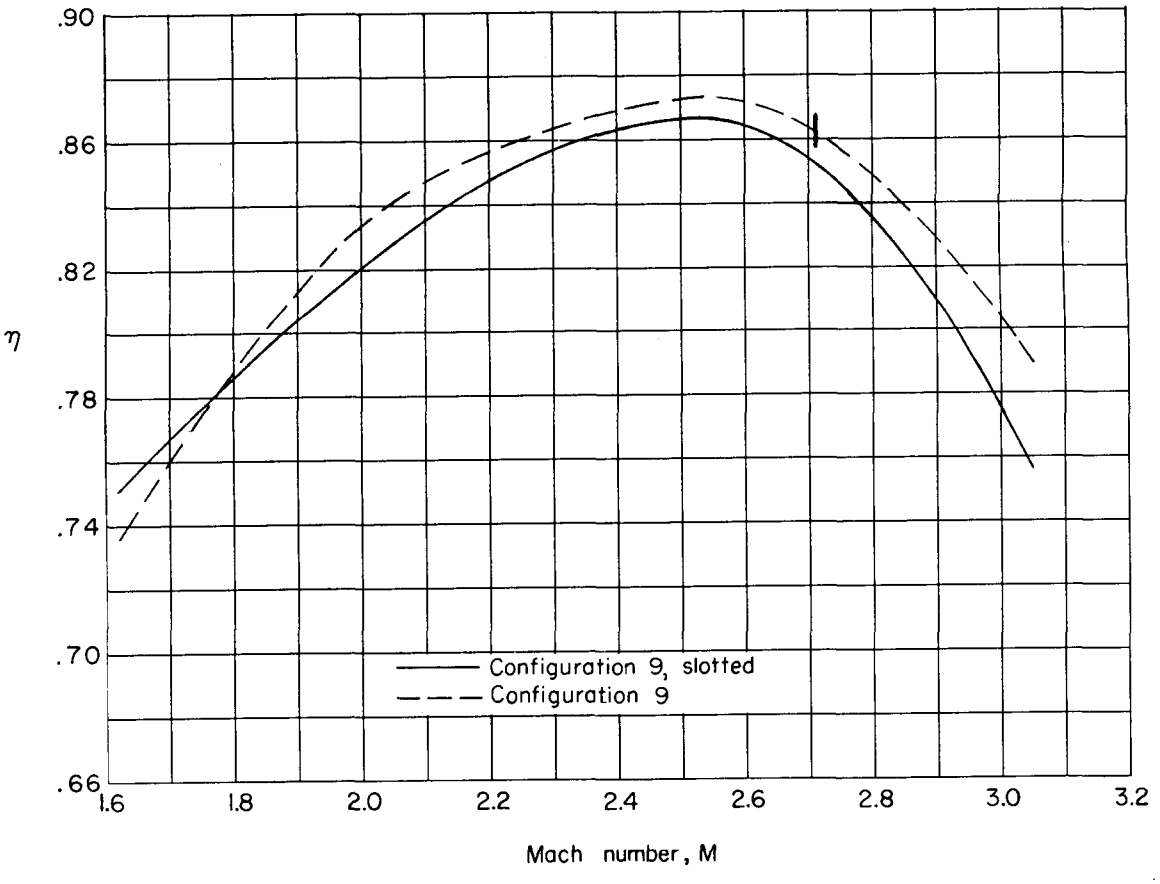

(b) Comparison of configuration 9 and configuration 9 slotted.

Figure 13.- Continued.

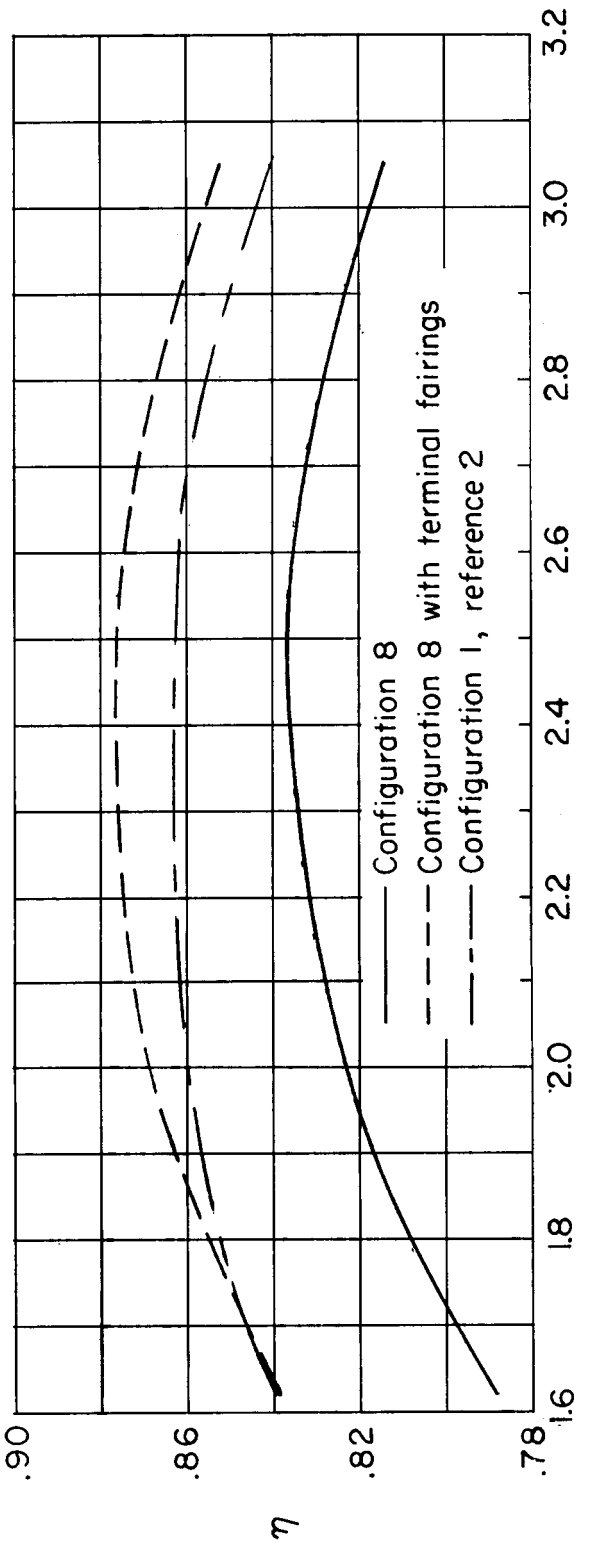

(c) Comparison of configuration 8 and configuration 8 with terminal fairings.

Figure 13.- Concluded.